1 **RNA-protein interaction analysis of SARS-CoV-2 5'- and 3'-untranslated**

2 **regions identifies an antiviral role of lysosome-associated membrane protein-2**

3

4 Rohit Verma[1,4], Sandhini Saha[2,4], Shiv Kumar[1], Shailendra Mani[3], Tushar Kanti Maiti[2], Milan

5 Surjit[1]*

6

7 [1]Virology Laboratory, Translational Health Science and Technology Institute, NCR Biotech

8 Science Cluster, Faridabad, 121001, Haryana, India.

9

10 [2]Laboratory of functional proteomics, Regional Centre for Biotechnology, NCR Biotech

11 Science Cluster, Faridabad, 121001, Haryana, India.

12

13 [3]Translational Health Science and Technology Institute, NCR Biotech Science Cluster,

14 Faridabad, 121001, Haryana, India.

15

16

17

18

19

20 [4]contributed equally

21

22 * Correspondence: milan@thsti.res.in

23

24

25

26

27

28 **Keywords:** SARS CoV-2; 5'-UTR; 3-UTR; RNA-protein interaction network; Coronavirus;

29 Virus-host interaction; Lamp2; Autophagy

30

31

32

33

34

35

36

Abstract

Severe acute respiratory syndrome-coronavirus-2 (SARS-CoV-2) is a positive-strand RNA virus. Viral genome is capped at the 5'-end, followed by an untranslated region (UTR). There is poly-A tail at 3'-end, preceded by an UTR. Self-interaction between the RNA regulatory elements present within 5'- and 3'-UTRs as well as their interaction with host/virus-encoded proteins mediate the function of 5'- and 3'-UTRs. Using RNA-protein interaction detection (RaPID) assay coupled to liquid chromatography with tandem mass-spectrometry, we identified host interaction partners of SARS-CoV-2 5'- and 3'-UTRs and generated an RNA-protein interaction network. By combining these data with the previously known protein-protein interaction data proposed to be involved in virus replication, we generated the RNA-protein-protein interaction (RPPI) network, likely to be essential for controlling SARS-CoV-2 replication. Notably, bioinformatics analysis of the RPPI network revealed the enrichment of factors involved in translation initiation and RNA metabolism. Lysosome-associated membrane protein-2a (Lamp2a) was one of the host proteins that interact with the 5'-UTR. Further studies showed that Lamp2 level is upregulated in SARS-CoV-2 infected cells and overexpression of Lamp2a and Lamp2b variants reduced viral RNA level in infected cells and vice versa. In summary, our study provides an useful resource of SARS-CoV-2 5'- and 3'-UTR binding proteins and reveal the antiviral function of host Lamp2 protein.

74 **Importance**

75 Replication of a positive-strand RNA virus involves an RNA-protein complex consisting of

76 viral genomic RNA, host RNA(s), virus-encoded proteins and host proteins. Dissecting out

77 individual components of the replication complex will help decode the mechanism of viral

78 replication. 5'- and 3'-UTRs in positive-strand RNA viruses play essential regulatory roles in

79 virus replication. Here, we identified the host proteins that associate with the UTRs of SARS-

80 CoV-2, combined those data with the previously known protein-protein interaction data

81 (expected to be involved in virus replication) and generated the RNA-protein-protein

82 interaction (RPPI) network. Analysis of the RPPI network revealed the enrichment of factors

83 involved in translation initiation and RNA metabolism, which are important for virus

84 replication. Analysis of one of the interaction partners of the 5'-UTR (Lamp2a) demonstrated

85 its antiviral role in SARS-CoV-2 infected cells. Collectively, our study provides a resource of

86 SARS-CoV-2 UTR-binding proteins and identifies an antiviral role of host Lamp2a protein.

87

88

89

90

91

92

93

94

95

96

97

98

99

100

101

102

103

104

105

106

107

108

109

110

Introduction

111   **Introduction**

112   In December 2019, a highly pathogenic coronavirus was identified in the Wuhan city, China,

113   which was named as 2019-nCoV/SARS-CoV-2 (1,2,3). Since then, the virus has spread

114   globally and World health organization (WHO) has classified the outbreak as a pandemic.

115   SARS-CoV-2 belongs to the family of *Coronaviridae*. Coronaviruses are known to be present

116   in animals and humans for a long time, usually resulting in respiratory and intestinal

117   dysfunction in the host (4). Until the emergence of Severe acute respiratory syndrome

118   coronavirus (SARS-CoV) in 2002, coronaviruses were not considered to be a significant

119   threat to human health (5). However, within last 18 years since the SARS outbreak, three

120   major human coronavirus outbreaks have occurred, suggesting that highly pathogenic

121   human coronaviruses are evolving fast. Considering the severity of the current SARS-CoV-2

122   pandemic, there is an urgent need to understand the life cycle and pathogenetic mechanism

123   of the virus. Since all coronavirus genomes share significant homology, the knowledge

124   obtained from the study of SARS-CoV-2 genome will be useful to formulate a long-term

125   action plan to deal with the current as well as future coronavirus outbreaks.

126   Coronaviruses are positive strand RNA viruses. Viral genome serves as the template for

127   synthesis of antisense strand, production of proteins involved in replication as well as

128   assembly of the progeny virions (6). Viral genome is capped at the 5'-end and poly

129   adenylated at the 3'-end. 5' and 3'-ends of the genome contain noncoding sequences, also

130   known as untranslated regions (UTRs). 5'- and 3'-UTRs in the positive strand of RNA

131   viruses play essential regulatory roles in virus replication, enhancing the stability of the viral

132   genomic RNA, host immune modulation and encapsidation of the viral genome into the

133   nucleocapsid core. Additionally, cis-acting regulatory elements are present within the coding

134   regions of the positive and negative strand (replication intermediate) of the viral genome.

135   These regulatory RNA elements also play significant roles in the life cycle and pathogenesis

136   of the virus. Intraviral interactions between regulatory RNA elements of the virus and

137   intraviral as well as virus-host RNA-protein interactions control the function of the 5'-, 3'-

138   UTRs and internal cis-acting RNA elements of the virus (7, 8).

139   SARS-CoV-2 contains a 260-nucleotide long 5'-UTR and a 200 nucleotide long 3'-UTR.

140   These UTRs show considerable homology with the 5'- and 3'-UTRs of other beta

141   coronaviruses such as SARS and SARS related beta coronaviruses (9). Distinct stem loops

142   and secondary structures within the UTRs are known to mediate their regulatory function.

143   Notably, stem loop I and stem loop II (SL-I and SL-II) of the 5'-UTR are important for long

144   range interaction and subgenomic RNA synthesis, respectively. SL-III contains the

145   translation-regulatory sequence (TRS), which is essential for the discontinuous transcription

146   of ORF1ab. SL-5 is crucial for the viral RNA packaging and translation of the ORF1ab

147   polyprotein (10, 11, 12).

4

148 The 3'-UTR of coronaviruses is important for viral replication (RNA synthesis and

149 translation). It contains a hyper variable region (HVR) which, has been shown to be

150 important for pathogenesis of mouse hepatitis virus (MHV). HVR contains a stem loop II-like

151 motif (S2M) that associates with host translation factors (13). S2M motif is also present in

152 the 3'-UTR of SARS-CoV-2 (9).

153 Interaction of host proteins with the 5'- and 3'-UTRs of viral genomic RNA is important for

154 replication and pathogenesis of many RNA viruses. Interaction of polypyrimidine tract

155 binding protein (PTB) with the 5'-UTR-TRS of MHV is known to control transcription of the

156 viral RNA (14, 15, 16). Further, RNA helicases such as DDX1, DHX15; proteins involved in

157 translation regulation such as eIF1α, eIF3S10; proteins involved in cytoskeleton movement

158 such as tubulin, Annexin A2, moesin as well as GAPDH (glyceraldehyde 3-phosphate

159 dehydrogenase) is known to associate with the 5'-UTR of few coronaviruses (7, 17). 3'-UTR

160 of MHV associates with hnRNPA1 and modulate viral replication (18). Poly-A binding protein

161 (PABP), transcriptional activator p100 (SND1), heat shock proteins (HSP40, HSP 60, HSP

162 70) associate with the 3'-UTR of MHV (19). Functional significance of some these

163 interactions are known (8).

164 Despite general acceptance of the importance of the 5'- and 3'-UTRs of RNA viruses in

165 controlling their replication and pathogenesis, no systematic study has been under taken to

166 elucidate the molecular composition of the RNA-protein complex assembled at the 5'- and

167 3'-UTRs of SARS-CoV-2 and function of 5'- and 3'-UTRs of SARS CoV-2.

168 We employed RNA-protein interaction detection (RaPID) assay coupled to liquid

169 chromatography with tandem mass spectrometry (LC-MS-MS) to identify the repertoire of

170 host proteins that interact with the SARS-CoV-2 5'- and 3'-UTR (20). These datasets were

171 used to construct the virus-host RNA-Protein-protein interaction (RPPI) network. *In silico*

172 analyses of the RPPI network revealed enrichment of proteins involved in multiple processes

173 such as Cap-dependent translation and RNA metabolism. Further studies revealed an

174 antiviral role of LAMP2 during SARS-CoV-2 infection. Functional significance of these

175 findings in SARS-CoV-2 replication and pathogenesis is discussed.

176

177 **Results**

178 **Identification of host proteins that interact with the 5'- and 3'-UTRs of SARS-CoV-2**

179 **genomic RNA.**

180 300 nucleotides from the 5'-end (denoted as 5'-300 RNA) and 203 nucleotides form the 3'-

181 end (3'-203 RNA) of the SARS-CoV-2 genomic RNA (Wuhan isolate), which includes the 5'-

182 and 3'-UTRs, respectively (nucleotides 1-264 and 29676-29878 in the viral genome), were

183 cloned into the pRMB vector in between the BirA Ligase binding stem loop (SL-A and SL-B)

184 sequences (Fig 1A-C). 5'- and 3'-UTRs consist of 264 and 228 nucleotides, respectively.

5

185 Extra bases were included at the 5'-end to ensure that stem loops in the predicted

186 secondary structures of the 5'-UTR remain intact in the hybrid RNA (Fig 1A). Eight Adenine

187 residues were retained at the 3'-end (Fig 1B). "mfold" mediated comparison of the secondary

188 structures of the 5'-300 and 3'-203 RNA sequences with and without BirA ligase binding

189 stem loop RNA sequences indicated that secondary structures of viral 5'-UTR and 3'-UTR

190 and BirA binding stem loops (SL-A and SL-B) are not disturbed in the hybrid RNA sequence

191 (compare SL-I to SL-Vc in the 5'-300 RNA and SL-A and SL-B in Fig 1A and S1 Fig;

192 compare SL-I to SL-IV and SL-A and SL-B in Figure 1B and S2 Fig). RaPID (RNA-Protein

193 interaction detection) assay was performed to identify the host proteins that interact with the

194 5'-300 and 3'-203 RNA in HEK293T cells. RaPID assay allows BirA ligase mediated *in vivo*

195 biotin labeling of host proteins that interact with the RNA sequence of interest cloned in

196 between the BirA ligase-binding RNA motifs. Biotinylated proteins are captured using

197 streptavidin agarose beads and identified by LC-MS-MS (Fig 1C, 20). Thus, both transiently

198 interacting and stably interacting proteins can be identified using this technique.

199 Expression of BirA ligase in HEK293T cells was confirmed by western blot using anti-HA

200 antibody that recognizes the HA-tag fused to the BirA ligase (Fig 1D). Optimal duration of

201 biotin treatment was selected through a time course analysis of biotin labeling, based on

202 which 18 hour labeling period was selected (Fig 1E). To test the functionality of the RaPID

203 assay, interaction between CUGBP1 protein and EDEN15 RNA was tested in the HEK293T

204 cells (20). Streptavidin pulldown of EDEN15 RNA interacting proteins, followed by western

205 blot using CUGBP1 antibody revealed the interaction between them, in agreement with

206 earlier report (Fig 1F, 20).

207 HEK293T cells expressing the SL-A-5'-300-SL-B or SL-A-3'-203-SL-B or SL-A-SL-B (pRMB)

208 was treated with Biotin, followed by pulldown of biotinylated proteins and LC-MS-MS

209 analysis. Biotin untreated cells were processed in parallel as control. Samples from three

210 independent experiments were run in triplicate. Pearson correlation analysis of MS data

211 demonstrated good correlation between replicates for individual biological samples (average

212 range: 0.5-0.98, Fig 2A). Specific and strong interaction partners of 5'-300 and 3'-203 RNAs

213 were identified in three steps (a) only those proteins having at least one biotinylated peptide

214 and a "Pep score" of 15 or more in all LC-MS samples were selected [(S3 Fig, S1 Table)

215 (21]; (b) subtraction of pRMB dataset from 5'-300 and 3'-203 datasets (Fig 2B); (c) from the

216 background subtracted dataset, only those proteins with minimum 2 unique peptides and

217 "Prot score" of 40 or more were considered for further analysis (Table 1).

218 Following similar protocol, in an unrelated study, we had identified host interaction partners

219 of the 3'-end (3'-UTR + adjacent 100 nucleotides) of the Hepatitis E virus (HEV) genomic

220 RNA (S2 Table). HEV is a positive strand RNA virus of the *hepeviridae* family and 3'-end of

221 the HEV harbors a secondary structure composed of multiple stem loops that have been

6

222   predicted to be important for viral replication (22). In order to further increase our confidence

223   in reliability of the RaPID technique, HEV 3'-end RNA interacting protein list was compared

224   to the SARS-CoV-2 5'-300 and 3'-203 RNA-interacting protein list. One protein (Histone

225   H3.1) was found to be common between the two datasets, indicating specificity of the

226   interacting proteins for the RNA baits. Therefore, using RaPID assay, 47 and 14 host

227   proteins were identified to interact with the 5'-300 and 3'-203 RNA, respectively (Table 1).

228   Out of these, 4 proteins (UBA1, GNL2, JAKMIP3 and YTHDF3) interacted with both 5'- and

229   3'-UTRs (Table 1, represented in bold font). A recent publication reported the atlas of

230   proteins bound to the SARS-CoV-2 RNA using the RAP-MS (RNA Antisense Purification

231   with Mass Spectrometry) technique (23). Comparison with that data identified 10 proteins to

232   be present in our 5'-300 dataset and 1 protein in the 3'-203 RNA binding protein data set

233   (Table 1). Based on human protein atlas data, except HIST3H3 and SLC25A31, rest 55

234   proteins are expressed in both human lungs and intestine (S3 Table).

235

236

237

238

239

240

241

242

243

244

245

246

247

248

249

250

251

252

253

254

255

256

Table 1. Host proteins that interact with the 5'-300 and 3'-203 RNA of SARS-CoV-2, identified by RaPID assay.

A. SARS-CoV-2 5'-300 RNA interacting host proteins

Gene Name	Description	Prot_Score	No. of biotinylated peptides	No. of unique peptides	Reported by Nora *et. al.*
HSPA1L	Heat shock 70 kDa protein 1-like	492	17	10	√
UBA1	Ubiquitin-like modifier-activating enzyme 1	380	6	4	-
MTHFD1	C-1-tetrahydrofolate synthase, cytoplasmic	372	21	8	-
HSPA1A	Heat shock 70 kDa protein 1A/1B	278	10	7	-
HIST3H3	Histone H3.1t	212	10	3	-
HIST1H3A	Histone H3.1	212	9	3	-
H3F3A	Histone H3.3	212	12	3	-
DIS3	Exome complex exonuclease RRP44	180	18	7	-
PHB2	Prohibitin-2	132	10	4	-
RPL7A	60S ribosomal protein L7a	120	29	13	√
LAMP2	Lysosome-associated membrane glycoprotein 2	119	4	2	-
RPLP2	60S acidic ribosomal protein P2	110	4	2	-
SNF8	Vacuolar-sorting protein SNF8	104	7	3	-
G3BP2	Ras GTPase-activating protein-binding protein 2	98	4	2	√
ABCE1	ATP-binding cassette sub-family E member 1	79	10	6	√
RPL13	60S ribosomal protein L13	78	7	4	√
CTTN	Src substrate cortactin	70	7	6	√
ABCF2	ATP-binding cassette sub-family F member 2	70	3	2	-
TPR	Nucleoprotein TPR	65	22	18	-
CKAP2	Cytoskeleton-associated protein 2	63	19	13	-
SNRNP200	U5 small nuclear ribonucleoprotein	61	23	16	√
EIF5B	Eukaryotic translation initiation factor 5B	61	30	12	-
SLC25A31	ADP/ATP translocase 4	60	12	7	-
PDHA1	Pyruvate dehydrogenase E1 component subunit alpha, somatic form, mitochondrial	60	12	5	√
GNL2	Nucleolar GTP-binding protein 2	55	13	10	-
GEMIN5	Gem-associated protein 5	55	5	3	-
JAKMIP3	Janus kinase and microtubule-interacting protein 3	54	7	5	-
GTSE1	G2 and S phase-expressed protein 1	54	9	4	-
MSH6	DNA mismatch repair protein Msh6	52	15	9	-
STIP1	Stress-induced-phosphoprotein 1	52	13	5	√
SEPT9	Septin-9	50	10	4	-
STMN2	Stathmin-2	49	8	6	-
FGFR1OP	FGFR1 oncogene partner	49	11	4	-
STMN1	Stathmin	49	6	4	-
MRPL40	39S ribosomal protein L40, mitochondrial	49	4	3	-
RANGAP1	Ran GTPase-activating protein 1	49	8	3	-
TTF2	Transcription termination factor 2	48	7	3	-
YTHDF3	YTH domain family protein 3	47	3	3	-
HDLBP	Vigilin	46	30	14	√
RAD50	DNA repair protein RAD50	46	21	13	-
AHNAK2	Protein AHNAK2	45	101	47	-
POLDIP3	Polymerase delta-interacting protein 3	45	8	5	-
ARHGAP21	Rho GTPase-activating protein 21	41	19	15	-
UTP3	Something about silencing protein 10	41	5	4	-
CDV3	Protein CDV3 homolog	41	3	3	-
HABP4	Intracellular hyaluronan-binding protein 4	41	7	2	-
FKBP4	Peptidyl-prolyl cis-trans isomerase FKBP4	40	7	4	-

B. SARS-CoV-2 3'-203 RNA interacting host proteins

Gene Name	Description	Prot_Score	No. of biotinylated peptides	No. of unique peptides	Reported by Nora *et. al.*
TUBA1A	Tubulin alpha-1A chain	536	5	4	√
UBA1	Ubiquitin-like modifier-activating enzyme 1	395	4	3	-
NASP	Nuclear autoantigenic sperm protein	218	3	3	-
RPL4	60S ribosomal protein L4	80	2	2	-
YTHDF3	YTH domain family protein 3	77	3	2	-
SRP54	Signal recognition particle 54 kDa protein	66	6	4	-
GNL2	Nucleolar GTP-binding protein 2	55	4	3	-
SCAPER	S phase cyclin A-associated protein in the ER	54	9	5	-
PLA2G4A	Cytosolic phospholipase A2	53	4	4	-
DCP1B	mRNA-decapping enzyme 1B	51	4	3	-
AGL	Glycogen debranching enzyme	50	10	4	-
JAKMIP3	Janus kinase and microtubule-interacting protein 3	47	12	5	-
NACAD	NAC-alpha domain-containing protein 1	44	14	4	-
DDX24	ATP-dependent RNA helicase DDX24	40	15	11	-

257

258 **Construction and analysis of the RNA-Protein-Protein interaction network at the 5'-**

259 **and 3'-ends of the SARS-CoV-2 genome**

260 5'-300 and 3'-203 RNA binding protein datasets were imported to "Cytoscape" to construct

261 the RNA-Protein-protein interaction networks (RPPI network) (24). 3'-203 interacting

262 proteins did not show any significant network characteristics (observed number of edges =1,

263 expected no. of edges =1, numbers of node =14 Average node degree = 0.143, average

264 clustering coefficient = 0.143 and PPI enrichment P value = 0.437) (Fig 2C). However, 5'-

265 300 and 5'-300+3'-203 interaction RPPI networks showed significant enrichment of

266 interactions [(5'-300 RPPI network characteristics: observed number of edges =27, expected

267 no. of edges =10, numbers of node =46, average node degree = 1.17, average clustering

268 coefficient = 0.311 and PPI enrichment P value = 3.64e-06); (5'-300+3'-203 RPPI network

269 characteristics: observed number of edges =39, expected no. of edges =14, numbers of

270 node =56, average node degree = 1.39, average clustering coefficient = 0.29 and PPI

271 enrichment P value = 1.27e-08)]. Note that, based on the above network parameters, 5'-

272 300+3'203 RPPI network is stronger than the 5'-300 network (Fig 2D, 2E).

273 Recently protein interaction map of SARS-CoV-2 has been reported (25). Since RNA-protein

274 complex assembled at the 5'- and 3'-UTR as well as Viral RNA-dependent RNA polymerase

275 (RdRp)-associated protein complex are known to drive the viral replication process in

276 positive strand RNA viruses, we combined the 5'-300+3'-203 RPPI dataset and previously

277 reported PPI dataset (only the subset of PPI proposed by Gordon and coworkers to be

278 involved in viral replication) to generate an integrated RPPI network of SARS-CoV-2

279 replication machinery (S4 Fig). As expected, the integrated RPPI network showed

280 significantly higher PPI enrichment compared to replication PPI alone [(Integrated RPPI

281 network characteristics: observed no. of edges =328, expected no. of edges =152, number

282 of nodes =196, average node degree = 3.35, average clustering coefficient = 0.492 and PPI

283 enrichment P value = 1.0e-16); (replication PPI network characteristics: observed no. of

284 edges =191, expected no. of edges =78, numbers of nodes = 143, average node degree =

285 2.67, average clustering coefficient = 0.501 and PPI enrichment P value = <1.0e-16)] (S4A

286 and S4B Figs).

287 Next, gene ontology (GO) and Reactome pathway analysis of the RPPI network was

288 performed using "GSEA tool" to determine the significantly enriched processes/pathways

289 (S5 and S6 Figs) (26, 27). Of note, proteins involved in intracellular transport, translation

290 initiation, amide biosynthetic pathway and mRNA metabolism were enriched in the GO-

291 Biological processes category (Table 2A). Similarly, proteins involved in cellular response to

292 external stimuli, HSP 90 chaperones for steroid hormone receptors, RNA metabolism,

293 translation, Influenza infection, infectious disease, cell cycle etc. were enriched in Reactome

294 pathway analysis (Table 2A).

295   Since, 5'- and 3'-UTRs are well conserved, drugs directly targeting the UTRs or acting upon

296   the proteins that interact with the UTRs may function as potent antivirals by inhibiting the

297   viral replication process. A search for known drugs against the 57 RNA binding proteins

298   listed in Table 1 identified six proteins (RPL13, PDHA1, HABP4, MTHFD1, TUBA1A,

299   PLA2G4A), against whom known drugs exist (Table 2B). Notably, Thalidomide, which

300   targets RPL13, is being tested in clinical trial to evaluate its efficacy as an anti-inflammatory

301   therapeutic in COVID-19 patients (28). C-1-tetrahydrofolate synthase (MTHFD1) is the target

302   of Tetrahydrofolic acid or vitamin B9, which is being used as a supplement in CoVID-19

303   treatment (29). Phospholipase A2 (PLA2G4A) is the target of steroid drug Fluticasone

304   propionate. A recent report shows the ability of another steroid drug "Ciclesonide" to block

305   SARS-CoV-2 replication by targeting its replication-transcription complex (30).

306

307

308

309

310

311

312

313

314

315

316

317

318

319

320

321

322

323

324

325

326

327

328

329

Table 2 : Gene ontology and Reactome pathway analyses of SARS-CoV-2 5'-300 and 3'-203 RNA-protein interaction network and identification of potential drug targets.

A. Gene ontology and Reactome pathway analysis of SARS-CoV-2 5'-300 and 3'-203 RNA-protein interaction network (Top 10 processes/pathways)

Gene Set Name	Observed gene count	p-value	Gene names
Gene Ontology (Biological Process)			
GO_INTRACELLULAR_TRANSPORT	19	1.87E-12	*TPR, ABCE1, RPL7A, RPLP2, RPL13, RPL4, POLDIP3, SRP54, LAMP2, CTTN, PHB2, SNF8, HSPA1L, GTSE1, RANGAP1, NACAD, GEMIN5, TUBA1A, ARHGAP21*
GO_INTRACELLULAR_PROTEIN_TRANSPORT	16	5.32E-12	*TPR, ABCE1, RPL7A, RPLP2, RPL13, RPL4, POLDIP3, SRP54, LAMP2, CTTN, PHB2, SNF8, HSPA1L, GTSE1, RANGAP1, NACAD*
GO_TRANSLATIONAL_INITIATION	9	8.13E-12	*TPR, ABCE1, RPL7A, RPLP2, RPL13, RPL4, YTHDF3, HABP4, EIF5B*
GO_AMIDE_BIOSYNTHETIC_PROCESS	14	2.51E-11	*TPR, ABCE1, RPL7A, RPLP2, RPL13, RPL4, POLDIP3, GEMIN5, YTHDF3, HABP4, EIF5B, MRPL40, PDHA1, MTHFD1*
GO_PROTEIN_CONTAINING_COMPLEX_SUBUNIT_ORGANIZATION	18	1.38E-10	*TPR, ABCE1, SRP54, LAMP2, CTTN, GEMIN5, MRPL40, HSPA1A, SNRNP200, G3BP2, STMN2, STMN1, FKBP4, H3-3A, CKAP2, NASP, H3C1, H3-4*
GO_MRNA_METABOLIC_PROCESS	13	2.80E-10	*RPL7A, RPLP2, RPL13, RPL4, POLDIP3, GEMIN5, YTHDF3, HABP4, HSPA1A, SNRNP200, DCP1B, DIS3, TTF2*
GO_PEPTIDE_BIOSYNTHETIC_PROCESS	12	6.54E-10	*TPR, ABCE1, RPL7A, RPLP2, RPL13, RPL4, POLDIP3, GEMIN5, YTHDF3, HABP4, EIF5B, MRPL40*
GO_CELLULAR_AMIDE_METABOLIC_PROCESS	14	9.20E-10	*TPR, ABCE1, RPL7A, RPLP2, RPL13, RPL4, POLDIP3, GEMIN5, YTHDF3, HABP4, EIF5B, MRPL40, PDHA1, MTHFD1*
GO_CELLULAR_MACROMOLECULE_LOCALIZATION	17	1.32E-09	*TPR, ABCE1, RPL7A, RPLP2, RPL13, RPL4, POLDIP3, SRP54, LAMP2, CTTN, PHB2, SNF8, HSPA1L, GTSE1, RANGAP1, NACAD, SEPTIN9.*
GO_PEPTIDE_METABOLIC_PROCESS	12	4.67E-09	*TPR, ABCE1, RPL7A, RPLP2, RPL13, RPL4, POLDIP3, GEMIN5, YTHDF3, HABP4, EIF5B, MRPL40*
Reactome pathway			
REACTOME_CELLULAR_RESPONSES_TO_EXTERNAL_STIMULI	14	1.40E-13	*HSPA1A, RPL4, RPL7A, RPL13, RPLP2, TPR, TUBA1A, FKBP4, HSPA1L, STIP1, H3C1, H3-3A, H3-4, RAD50*
REACTOME_METABOLISM_OF_RNA	12	1.60E-10	*HSPA1A, RPL4, RPL7A, RPL13, RPLP2, TPR, DIS3, UTP3, GEMIN5, DCP1B, POLDIP3, SNRNP200*
REACTOME_HSP90_CHAPERONE_CYCLE_FOR_STEROID_HORMONE_RECEPTORS_SHR_	5	1.93E-08	*HSPA1A, TUBA1A, FKBP4, HSPA1L, STIP1*
REACTOME_INFLUENZA_INFECTION	6	1.01E-07	*HSPA1A, RPL4, RPL7A, RPL13, RPLP2, TPR*
REACTOME_TRANSLATION	7	2.11E-07	*RPL4, RPL7A, RPL13, RPLP2, SRP54, EIF5B, MRPL40*
REACTOME_INFECTIOUS_DISEASE	10	3.64E-07	*HSPA1A, RPL4, RPL7A, RPL13, RPLP2, TPR, TUBA1A, H3C1, RANGAP1, SNF8*
REACTOME_RRNA_PROCESSING	6	4.86E-07	*RPL4, RPL7A, RPL13, RPLP2, DIS3, UTP3,*
REACTOME_CELL_CYCLE	9	5.64E-07	*TPR, TUBA1A, H3C1, H3-3A, H3-4, RAD50, RANGAP1, CEP43, GTSE1*
REACTOME_SRP_DEPENDENT_COTRANSLATIONAL_PROTEIN_TARGETING_TO_MEMBRANE	5	6.08E-07	*RPL4, RPL7A, RPL13, RPLP2, SRP54*
REACTOME_EUKARYOTIC_TRANSLATION_INITIATION	5	8.19E-07	*RPL4, RPL7A, RPL13, RPLP2, EIF5B*

B. Known drugs targeting SARS-CoV-2 5'-300 and 3'-203 RNA interacting host proteins

Viral RNA binding protein	Gene name	Drug name
5'-300 RNA interacting host proteins	*RPL13*	Thalidomide
	PDHA1	NADH
	HABP4	Hyaluronan
	MTHFD1	Tetra hydro folic acid
3'-203 RNA interacting host proteins	*TUBA1A*	Albendazole, Vinblastine, Mebendazole
	PLA2G4A	Fluticasone Propionate

330

11

Lamp2 is a host restriction factor against SARS CoV-2

Lamp2a (CD107b) was identified as an interaction partner of the 5'-300 RNA in RaPID assay. LAMp2a is the receptor for chaperone mediated autophagy and recent studies have proposed a role of autophagy in SARS-CoV-2 pathogenesis (31). Hence, significance of the interaction between 5'-300 RNA and Lamp2a in SARS-CoV-2 life cycle was investigated using mammalian cell culture-based infection model of SARS CoV-2.

Vero E6 cell based infection model of SARS-CoV-2 was established to investigate the role of Lamp2a in SARS-CoV-2 life cycle. Productive infection of Vero E6 cells with SARS-CoV-2 was detected by immunofluorescence staining of the viral nucleocapsid (N) protein at 48 hour post-infection using anti-N antibody (Fig 3A). N- staining was not observed in uninfected cells (Fig 3A). Expression of N protein was also detected by western blot using anti-N antibody, 48-hour post infection (Fig 3B, upper panel). An aliquot of the samples were immunoblotted with anti-GAPDH antibody to monitor equal loading of protein in uninfected and infected cells (Fig 3B, lower panel). Next, level of viral RNA in the culture media (from released virus) and inside the cells (intracellular) was measured by the quantitative real time PCR (QRT-PCR) analysis of 48 hour and 72 hour SARS-CoV-2 infected samples using SYBR green based method. QRT-PCR detection of RNA polymerase II (RP II) and RNase P (RP) served as normalization control for intracellular and secreted RNA quantity, respectively. An increase in viral RNA level was observed in 72 hour infected intracellular and secreted samples, compared to 48 hour infected sample, indicating productive infection of Vero E6 cells with SARS-CoV-2 (Fig 3C). Aliquots of the RNA from culture media was also used in Taqman probe based one step QRT-PCR analysis using primers and probes recommended by the Centre for disease control (CDC), USA, for detection of SARS-CoV-2 (Fig 3D). Both SYBR green and Taqman QRT-PCR methods showed comparable result, hence SYBR green method was followed in subsequent experiments. Collectively, these data demonstrate the establishment of Vero E6 infection model of SARS-CoV-2 in our experimental setups.

A fluorescence *in situ* hybridization (FISH) was conducted to monitor the interaction between 5'-300 region of viral genome and Lamp2 in SARS-CoV-2 infected Vero E6 cells. Lamp2 (green) and 5'-300 RNA specific probe (red) colocalized (indicated by yellow), suggesting their interaction (Fig 3E). Next, smart pool SiRNA targeting Lamp2 RNA was used to deplete Lamp2 protein in veroE6 cells. Western blot of Vero E6 whole cell extract after 48 and 72 hours of Lamp2 siRNA transfection demonstrated that siRNA was effective in reducing total Lamp2 level by >90% in siRNA transfected cells (Fig 3F, upper panel). GAPDH was used as a loading control (Fig 3F, lower panel). QRT-PCR of 72 hour siRNA transfected SARS-CoV-2 infected Vero E6 cells (analyzed 48 hour post-infection) revealed an increase in viral RNA level in both culture medium (Fig 3G) and inside the cells (Fig 3H).

12

368 Results obtained in Vero E6 cells were further verified in a human hepatoma (huh7) cells-
369 based infection model of SARS CoV-2. Recent reports have shown the utility of Huh7 cells
370 as a viable model for SARS-CoV-2 infection (23, 32). Infection of Huh7 cells by SARS-CoV-
371 2 was confirmed by measuring the level of viral RNA inside the cells (intracellular) as well as
372 in the culture medium (secreted). As expected, an increase in viral RNA level at 72 hour
373 post-infection period (compared to 48 hour post-infection) indicated productive infection of
374 these cells (S7A Fig). Further, western blot using anti-N antibody confirmed N-expression in
375 infected samples (72 hour, S7B Fig). Lamp2 siRNA transfection reduced the corresponding
376 protein level by >90% in Huh7 cells (S7C Fig). A significant increase in viral RNA level was
377 observed in both culture medium and intracellular samples in 72 hour Lamp2 siRNA
378 transfected and 48 hour SARS-CoV-2 infected Huh7 cells (S7D and 7E Figs).
379 Lamp2 is present in three different forms in mammalian cells that include Lamp2a, Lamp2b
380 and Lamp2c, produced through alternative splicing (33). Lamp2a and Lamp2b are the major
381 forms. Lamp2a is highly expressed in lungs, liver and placenta. Lamp2b varies from Lamp2a
382 in the last 11 amino acids at its C-terminal sequence and it is highly expressed in Skeletal
383 muscle (34). Lamp2 antibody used in this study recognizes all three Lamp2 variants.
384 Next, the effect of overexpression of each Lamp2 isoform on SARS-CoV-2 replication was
385 tested in Vero E6 cells. Overexpression of Lamp2a and Lamp2b significantly reduced the
386 viral RNA level whereas Lamp2c overexpression did not alter viral RNA level at 48 hour
387 post-infection, both in culture medium (Fig 4A) and intracellular samples (Fig 4B). Lamp2a, b
388 and c overexpression was confirmed in aliquots of the sample using anti-lamp2 antibody,
389 which recognizes all Lamp2 variants (Figs 4C-4E) as well as using anti-HA antibody (for
390 Lamp2a). Similar results were obtained in Huh7 cell-based model of SARS-CoV-2 infection
391 (S7F-7J Figs). Note that overexpressed Lamp2a and Lamp2b could be detected using both
392 anti-HA and anti-Lamp2 antibodies in Huh7 cells but overexpressed Lamp2b could be
393 detected using only anti-Lamp2 antibody in Vero E6 cells. Also note that no epitope tag is
394 present in Lamp2c expression clone. Hence it was detected using anti-Lamp2 antibody.
395 In order to test if the observed reduction in viral RNA levels were specific to Lamp2, effect of
396 Lamp1 depletion on SARS-CoV-2 replication was evaluated. Western blot using anti-Lamp1
397 antibody showed ~90% reduction in Lamp1 protein level in siRNA transfected Huh7 cells at
398 48 hour and 72 hour time points (Fig 4F). QRT-PCR analysis of Lamp1 SiRNA treated
399 SARS-CoV-2 infected cells did not show any significant change in the level of viral RNA in
400 culture medium (Fig 4G) and intracellular samples (Fig 4H).
401
402 **Increased Lamp2 protein level in SARS-CoV-2 infected cells does not promote**
403 **autophagolysosome formation**

404 Lamp2a is the receptor for chaperone mediated autophagy and silencing of Lamp2

405 expression promoted SARS-CoV-2 replication. Therefore, we next measured the status of

406 autophagy in SARS-CoV-2 infected cells. An increase in the level of LAMP2, LC3 II and p62

407 protein was observed in the SARS-CoV-2 infected Vero E6 and Huh7 cells (Fig 5A). No

408 change in the level of Lamp1 was observed (Fig 5A). Treatment of SARS-CoV-2 infected

409 Vero E6 and Huh7 cells with 3 methyl adenine (3-MA), which is a specific inhibitor of

410 autophagy, completely diminished viral RNA in both culture medium and intracellular

411 samples (Fig 5B-E). Next, Immunofluorescence staining of Lamp2 (green) and LC3 (Red)

412 proteins was performed in SARS-CoV-2 infected or uninfected Vero E6 cells. Formation of

413 autophagolysosome is indicated by colocalization of Lamp2 and LC3, which forms "yellow"

414 color puncta in dual stained cells (35). No increase in autophagolysosome formation was

415 visible in SARS-CoV-2 infected Vero E6 cells (Fig 5F).

416

417 **Discussion**

418 In this study, we identified 57 host proteins that interact with the 5'- and 3'-ends of the

419 SARS-CoV-2 genomic RNA, combined those dataset with the PPI dataset proposed to be

420 involved in viral replication and constructed an RPPI network, which is likely to be

421 assembled during the replication of SARS-CoV-2. Interaction of 5'- and 3'- regulatory

422 elements with virus-encoded and host proteins mediate their function. Since 5'- and 3'-

423 regulatory elements are known to play indispensable roles in replication process of RNA

424 viruses, identification of the components of the above-mentioned RNA-protein complex

425 paves the way for designing novel antiviral therapeutic strategies against the SARS-CoV-2.

426 Among the viral proteins, N protein of MHV, TGEV and SARS-CoV binds to the 5'-UTR (8).

427 NSP8 and Nsp9 of MHV binds to the 3'-UTR (36). Many host proteins are known to bind to

428 the 5'- and 3'- UTR of viral genome and regulate virus replication (7). During the course of

429 this study, Schmidt *et al.* identified a number of host proteins that bind to SARS-CoV-2 RNA

430 in infected Huh7 cells using the RAP-MS technique (23). Comparison of their dataset to that

431 of this study identified 11 common proteins. This study identified additional 46 host proteins

432 that associate with 5'- and 3'-UTRs of the SARS-CoV-2 RNA. This may be attributed to the

433 ability of RaPID technique to detect both stable and transient as well as direct and indirect

434 (as a protein complex) RNA-protein interactions. Specificity of the data is evident from the

435 fact that only one protein (HIST1H3) is common between SARS-CoV-2 and HEV RPPI

436 datasets. Note that similar to SARS CoV-2, HEV is also a positive strand RNA Virus, which

437 contains a capped 5'-end, followed by a 5'-UTR and poly A tail preceded by a 3'-UTR (37).

438 Therefore, some aspects of replication process might be similar in both viruses.

439 In addition to lungs, SARS-CoV-2 has been reported to cause enteric infection. High level of

440 ACE2 is expressed in the intestinal epithelial cells and COVID-19 patients suffer from

441　gastrointestinal disorders (4). Therefore, we hypothesized that host proteins that are crucial

442　for the survival of the virus should be expressed in both lung and intestinal epithelium cells.

443　Comparison of expression of 5'-300 and 3'-203 RNA binding proteins in lung and intestinal

444　epithelium cells showed that 55 out of 57 proteins are expressed in both tissues, in support

445　of the above statement.

446　Among the 5'- and 3'-UTR interacting host proteins, known drugs exist against RPL13,

447　PDHA1, HABP4, MTHFD1, TUBA1A and PLA2G4A. Interestingly, some of the drugs being

448　used/tested in COVID-19 patients such as Thalidomide and Ciclosonide act by targeting two

449　of the above-mentioned proteins. Nevertheless, further studies are required to conclude if

450　those drugs act in COVID-19 patients by targeting the observed RNA-protein interaction or

451　through any other mechanism.

452　Gene ontology and Reactome pathway analysis of the SARS-CoV-2 5'- and 3'-UTR RPPI

453　datasets show an enrichment of proteins involved in different processes such as translation

454　initiation, RNA metabolism, infectious disease, which is expected. Therefore, the data

455　obtained by the RaPID assay is an useful resource for future studies related to the SARS

456　CoV-2. Comparison of SARS-CoV-2 5'-UTR and 3'-UTR interacting proteins obtained in the

457　RaPID assay with those shown in other positive strand RNA viruses reveal a similar profile

458　of many functional protein categories. Proteins belonging to the ribosome complex such as

459　RPL7a, RPLP2, RPL13, RPL4 and translation initiation factor such as eIF5B were found to

460　interact with the SARS-CoV-2 5'-and 3'-UTR. Being a capped RNA, SARS-CoV-2 genomic

461　RNA is supposed to utilize the canonical cap-dependent translation process for producing

462　viral proteins and above-identified host factors might be used by the virus for efficiently

463　translating its own RNA. Heat shock proteins of the HSP70 and HSP90 family are required

464　for maintenance of cellular homeostasis by virtue of their ability to recognize and fold or

465　remove unfolded proteins (38). They are also important for proper assembly and/or

466　disassembly of viral replication complex (39). They require the adapter protein STIP1 for

467　optimal activity. In the case of SARS CoV-2, HSP71, HSP71L and STIP1 were found to

468　interact with the 5'-UTR. Dead box RNA helicases such as DDX1 and DHX15 are known to

469　associate with the TRS in MHV (7). DDX24 was identified to interact with the 3'-UTR of

470　SARS CoV-2. DDX24 is known to associate with RNA and negatively regulate RIG-I-like

471　receptor signaling, resulting in inhibition of host antiviral response (40). Several proteins

472　encoded by the SARS-CoV-2 such as Nucleocapsid, ORF6 and ORF8 are known to inhibit

473　host antiviral response (41). Interaction of DDX24 with SARS-CoV-2 3'-UTR might be an

474　additional strategy to inhibit the host antiviral response. Further studies are required to

475　confirm the above hypothesis.

476　ATP-binding cassette subfamily E member 1 (ABCE1) is another important host protein that

477　interacts with the 5'-UTR. ABCE1 (RNAse L inhibitor) inhibits the activity of RNAse L, which

15

478   is activated by the host antiviral response mechanism in response to RNA virus infection or

479   IFN α/β stimulation (42). Active RNAse L cleaves the viral RNA, which is prevented in the

480   presence of ABCE1. It will be interesting to explore the significance of 5'-UTR interaction

481   with ABCE1. Note that ABCE1 was also identified as a direct interaction partner of SARS-

482   CoV-2 RNA by Schmidt et al. (23). FKBP4 was also found to interact with the 5'-UTR. It is a

483   member of the immunophilin protein family and binds to immunosuppressants FK506 and

484   rapamycin (43). Further, Ras GTPase activating protein binding protein 2 (G3BP2), which is

485   key to stress granules formation, was found to interact with the 5'-UTR of SARS CoV-2.

486   G3BP1/2 has also been shown to bind to the N protein of SARS-CoV-2 (25). Stress granules

487   play key roles controlling viral infections (44). N protein of SARS-CoV-2 is predicted to

488   associate with the 5'-UTR. Hence, interaction of both N and 5'-UTR with G3BP2 may be an

489   important strategy of SARS-CoV-2 to modulate the function of stress granules in infected

490   cells. 5'-UTR was also found to interact with the exosome endoribonuclease RRP4, which is

491   involved in cellular RNA processing and degradation. The RNA exosome complex is a

492   quality control mechanism of the host that regulates mRNA turnover and degrades aberrant

493   RNAs. SARS-CoV-2 might be modulating this pathway for its own benefit.

494   5'-UTR was also found to interact with Lamp2a, which is another key protein involved in

495   quality control processes of the host. Lamp2a is the receptor for the chaperone mediated

496   autophagy (45). Our data shows an increase in autophagic flux in the SARS-CoV-2 infected

497   cells and significant reduction in viral RNA level by inhibition of autophagy. Therefore, it

498   appears that increased autophagic flux promotes SARS-CoV-2 replication, as seen in many

499   other RNA viruses (46). However, there was no change in autophagolysosome formation in

500   SARS-CoV-2 infected cells. Similar phenomenon is observed in the case of HCV infection

501   (47). Lack of Lamp2 protein increased the level of viral RNA in the SARS-CoV-2 infected

502   cells. Therefore, Lamp2a interaction with the 5'-UTR is unlikely to play a role in promoting

503   viral replication.

504   Lamp2b and Lamp2c isoforms are known to directly interact with RNA and DNA, leading to

505   RNautophagy/DNautophagy (48). Lamp2c is predominantly involved in importing nucleic

506   acids to lysosome for degradation (49). Lamp2 isoforms vary in their C-terminal region.

507   Although SARS-CoV-2 5'-UTR interacts with Lamp2a, SiRNA used in our study acts by

508   binding to the 5' end of the Lamp2 transcript. Therefore, it acts on all Lamp2 variants. The

509   antibody used in our study recognizes all Lamp2 isoforms. However, since Lamp2c

510   overexpression did not affect viral RNA level, it is unlikely that the observed increase in viral

511   RNA level in Lamp2 siRNA treated cells were attributed to a block in RNautophagy.

512   Lamp2a-5'UTR interaction may be involved in delivering viral RNA to endosome, for

513   recognition by TLR7, the sensor for ssRNA. Lamp2a and 5'-UTR interaction may also be

514   involved in sequestering away Lamp2a from inducing chaperone mediated autophagy. At

16

515 the same time, increased autophagic flux provides energy and prevents apoptosis of the

516 infected cells, which provides a favorable environment to the virus to complete its life cycle.

517 Further studies are required to understand the actual process. Nevertheless, the current

518 study identifies the repertoire of host proteins that associate with the SARS-CoV-2 5'- and

519 3'-UTR and demonstrate a prosurvival role of the host Lamp2 protein against the Virus.

520

521 **Materials and Methods**

522

523 **Plasmids and reagents**

524 Sequence corresponding to 1-300 nucleotides at the 5' end (5'-300) and 29676-29900 at the

525 3'end (3'-203) of the SARS CoV2 isolate Wuhan-hu-1 genome (Genbank: NC_045512) were

526 commercially synthesized and cloned into pUC57 vector (Genscript, New Jersey, USA).

527 RNA motif plasmid cloning backbone [(pRMB) (Addgene plasmid # 107253 ;

528 http://n2t.net/addgene:107253 ; RRID:Addgene_107253)], BASU RaPID plasmid (Addgene

529 plasmid # 107250 ; http://n2t.net/addgene:107250 ; RRID:Addgene_107250), RNA motif

530 plasmid EDEN15 (Addgene plasmid # 107252 ; http://n2t.net/addgene:107252 ;

531 RRID:Addgene_107252) were gifted by Paul Khavari. pCDNA Lamp2b was a gift from

532 Joshua Leonard (Addgene plasmid # 71292 ; http://n2t.net/addgene:71292 ;

533 RRID:Addgene_71292) and pCDNA lamp2c was a gift from Janice Blum (Addgene plasmid

534 # 89342 ; http://n2t.net/addgene:89342 ; RRID:Addgene_89342). pcDNA Lamp2a (Cat no.

535 HG29846-CY) was purchased from Sino Biologicals (Beijing, China). Anti-Lamp2 (Cat. No.

536 49067), anti-Lamp1 (Cat no. 9091), anti-LC3B (Cat no. 83506) and anti-P62 (Cat no. 8025s)

537 antibodies were from Cell signalling Technology (Massachusetts, USA). Anti-GAPDH

538 antibody (Cat No. SC-25778) was from Santacruz Biotechnology (Texas, USA). Anti-Flag

539 antibody (Cat no. A190-101) was from Bethyl laboratory (Texas, USA). Anti-CUGBP1

540 antibody (Cat no. STJ92521) was from St John's Laboratory, (London, UK). Goat anti-rabbit

541 IgG-HRP (Cat No. 4030-05) and Goat anti-mouse IgG-HRP (Cat No. 1030-05) was from

542 Southern Biotech (Alabama, USA). Goat anti-rabbit IgG Alexa fluor 488 (Cat no. A-11008),

543 goat anti-mouse IgG Alexa fluor 647 (A-21235) and Antifade gold with DAPI (P36931) was

544 from Thermo Fisher Scientific (Massachusetts, USA). 3-MA (Cat no. M9281) and Anti-HA

545 antibody (Cat no. A190-101) was from Sigma (Missouri, USA). Nontargeting siRNA (Cat no.

546 D-001810-10-20), Lamp1 siRNA (Cat no. L-013481-02-0005) and Lamp2 siRNA (Cat no. L-

547 011715-00-0005) were from Dharmacon (Colorado, USA).

548

549 **Mammalian cell culture and transfection**

550 Vero E6 and HEK 293T cells were obtained from ATCC (Virginia, USA). Huh7 cells have

551 been described (50). Cells were maintained in Dulbecco's modified Eagle medium (DMEM)

17

552   containing 10% Fetal bovine Serum (FBS), 50 I.U./mL Penicillin and Streptomycin, in 5%

553   CO_2. For plasmid transfection, cells were seeded at 70-80% confluency in DMEM+10% FBS

554   and incubated overnight. Next day, cells were transfected with desired plasmid DNA using

555   Lipofectamine 2000 transfection reagent (Life Technologies, California, USA) at 1:1 ratio,

556   following manufacturer's instruction. 6-8 hours post-transfection, culture medium was

557   replaced with fresh DMEM+10% FBS.

558   For experiments involving siRNA mediated gene silencing, Huh7 or Vero E6 cells were

559   seeded at 70-80% confluency on 12 well TC dishes and incubated overnight at 37^0C, 5%

560   CO_2. Next day, 25nmol siRNA was transfected into each well using 0.35 μl Dharmafect

561   transfection reagent, following manufacturer's instruction (Dharmacon, Colorado, USA). 18

562   hours post-transfection, culture medium was replaced with DMEM+10% FBS and cells were

563   maintained at 37^0C, 5% CO_2 until further manipulation.

564

565   **RaPID assay**

566   5'-300 and 3'-228 regions were PCR (Polymerase chain reaction) amplified from the pUC57

567   vector and cloned into RNA Motif plasmid cloning backbone vector (pRMB) at the BsmBI

568   restriction site using the following primers. 5'-300 FP: ATTAAAGGTTTATACCTTCCCAGG,

569   5'-300 RP: GTTTTCTCGTTGAAACCAGGG, 3'-203 FP: AATCTTTAATCAGTGTGTAACA,

570   3'-203 RP: TTTTTTTTGTCATTCTCCTAAG. Positive clones were checked by restriction

571   mapping and confirmed by DNA sequencing.

572   Production of 5'-300 and 3'-203 RNA from the pRMB constructs was verified by transfection

573   of pRMB 5'-300 and pRMB 3'-203 plasmids along with pRMB vector into HEK293T cells

574   followed by RT-PCR detection of the 5'-300 and 3'-203 RNA using above-mentioned primer

575   pairs. Expression of Bir*A ligase in HEK293T cells upon transfection of BASU plasmid was

576   verified by western blot (see Fig 1D). Time duration for biotin treatment were optimized by

577   co-transfection of RNA motif plasmid EDEN15 (pRMB EDEN15) and BASU plasmid in 6:1

578   ratio using Lipofectamine 2000 (1:1 ratio) into HEK293T cell. 42hour post transfection,

579   200μM biotin was added to the media and cells were incubated for 6, 12 and 18 hours. At

580   each time point, whole cell extract was prepared in 2X laemmli buffer and equal amount of

581   protein was resolved by 10% SDS- PAGE, followed by western blot using anti-Biotin

582   antibody (Fig 1E).

583   For verifying the interaction between EDEN 15 and CUGBP1 by RaPID assay, HEK293T

584   cells were transfected with (pRMB EDEN15) and BASU plasmids (6:1 ratio) using

585   Lipofectamine 2000 (1:1 ratio, Life Technologies, California, USA). 40 hours post-

586   transfection, culture medium was replaced and 200μM Biotin was added. 18 hours later,

587   cells were washed three times in PBS and lysed in prechilled RIPA buffer (150 mM NaCl,

18

588   1.0% NP-40, 0.5% sodium deoxycholate, 0.1% SDS, 50mM Tris, pH 8.0) supplemented with

589   protease and phosphatase inhibitor cocktail. The lysate was centrifuged at 14,000 × g for 45

590   min at 4^0C. Free biotin was removed by Macrosep Advance Spin Filter 3K MWCO 20 mL

591   (Cat no. 89131-974, VWR, USA). Aliquots of the samples were stored at -80^0C for use as

592   input in western blot. Protein concentration in each sample was determined using BCA

593   protein assay kit (Cat no. Thermo Fisher Scientific, Massachusetts, USA) and equal amount

594   of proteins were incubated with "MyOne Streptavidin C1" magnetic beads (Cat no. 65002,

595   Life Technologies, California, USA) on a rotator at 4^0C for 16 hours. Samples were washed

596   four times with washing buffer, 2X Laemmli buffer was added to the beads and incubated at

597   95^0C for 45 min. Both input and pull down samples were resolved by SDS-PAGE, followed

598   by western blot using anti-CUGBP1 and GAPDH antibodies. Goat anti-rabbit IgG HRP

599   conjugated secondary antibody was used to detect the protein bands by chemiluminescence

600   (Clarity ECL substrate, Cat no.170-5061, Biorad, California, USA).

601   For mass-spectrometry, clarified cell lysate was precipitated in acetone at -20^0C for 10 min,

602   followed by storage at -80^0C for 20 mins. The precipitates were solubilized in 8M urea. The

603   protein concentration was estimated by BCA protein assay kit (Thermo Fisher Scientific,

604   Massachusetts, USA).

605   *In-Solution Digestion and Peptide Separation:*

606   Equal amount of protein (10 mg) from each sample was treated with 10 mM DTT (56^0C, 30

607   min) and alkylated with 20 mM Iodoacetamide (IAA) at room temperature, 60 min, dark).

608   Trypsin (Cat no. T1426, Thermo Fisher Scientific, Massachusetts, USA) was added to the

609   samples at 1:20 (w/w) ratio and incubated at pH 8, 37^0C for 24 h. Next, 1% formic acid was

610   added to the samples and peptides were desalted using a SecPak C18 cartridge (Cat no.

611   WAT020515, Waters, Massachusetts, USA) and subsequently lyophilised in a Speed Vac.

612   High capacity streptavidin agarose resins (Cat no. 20361, Thermo Fisher Scientific,

613   Massachusetts, USA) were used to pull down the biotinylated peptides. The beads were

614   washed in binding buffer (50mM Na_2HPO_4, 150mM NaCl; pH 7.2) before use.

615   Lyophilised peptides were solubilized in 1 mL PBS and incubated with 150 μL washed

616   streptavidin agarose beads for 2 hour at room temperature. Beads were washed once in

617   1mL PBS, once in 1 mL washing buffer (5% acetonitrile in PBS) and finally washed once in

618   ultrapure water. Excess liquid was completely removed from the beads, and biotinylated

619   peptides were eluted by adding 0.3 mL of a solution containing 0.1% formic acid and 80%

620   acetonitrile in water by boiling at 95^0C for 5 min. A total of 10 elutions were collected and

621   dried together in a Speed Vac. Enriched peptides were desalted with C18 tips (Thermo

622   Fisher Scientific, Massachusetts, USA), and reconstituted with solvent A (2% (v/v)

623   acetonitrile, 0.1% (v/v) formic acid in water) for LC-MS/MS analysis.

624   *LC-MS/MS acquisition:*

19

625 LC−MS/MS experiments were performed using Sciex 5600$^+$ Triple-TOF mass spectrometer

626 coupled with ChromXP reversed-phase 3 μm C18-CL trap column (350μm × 0.5 mm, 120 Å,

627 Eksigent, AB Sciex, Massachusetts, USA) and nanoViper C18 separation column (75 μm ×

628 250mm, 3 μm, 100 Å; Acclaim Pep Map, Thermo Fisher Scientific, Massachusetts, USA) in

629 Eksigent nanoLC (Ultra 2D plus) system. The binary mobile solvent system was used as

630 follows: solvent C (2% (v/v) acetonitrile, 0.1% (v/v) formic acid in water) and solvent B (98%

631 (v/v) acetonitrile, 0.1% (v/v) formic acid). The peptides were separated at a flow rate of 200

632 nl/min in a 60 min gradient with total run time of 90 min. The MS data of each condition was

633 acquired in IDA (information-dependent acquisition) with high sensitivity mode. Each cycle

634 consisted of 250 and 100 ms acquisition time for MS1 (m/z 350−1250 Da) and MS/MS (100–

635 1800 m/z) scans, respectively, with a total cycle time of ~2.3s. Each condition was run in

636 triplicate.

637 *Protein Identification and Quantification:*

638 All raw files (.wiff) were searched using "ProteinPilot" software (version 4.5, SCIEX) with the

639 Mascot algorithm, for protein identification and semi quantitation against the

640 SwissProt_57.15 database (20266 sequences after Homo sapiens taxonomy filter). The

641 search parameters for identification of biotinylated peptides were as follows: (a) trypsin as a

642 proteolytic enzyme (with up to two missed cleavages); (b) peptide mass error tolerance of 20

643 ppm; (c) fragment mass error tolerance of 0.20 Da; and (d) carbamido-methylation of

644 cysteine (+57.02146 Da), oxidation of methionine (+15.99492 Da), deamination of NQ

645 (+0.98416) and biotinylation of lysine (+226.07759 Da) as variable modifications. Quality of

646 data between different samples and replicates were monitored by Pearson-correlation plot of

647 peptide intensity against each run.

648 *Data analysis:*

649 Proteins with at least one corrected biotinylated peptide and ≥ 15 PEP score were

650 considered to be identified successfully, extracted from the gaussian smooth curve. Next, all

651 data were analyzed using a web based tool, Bioinformatics & Evolutionary Genomics

652 (http://bioinformatics.psb.ugent.be/webtools/Venn/) to generate the venn diagram to identify

653 proteins that are unique interaction partner of 5'-300 and 3'-203 RNA. The background

654 subtracted dataset was sorted on the basis of following parameters (minimum 2 unique

655 peptides and "Prot score" of 40 or more) to generate the final list of proteins, which were

656 considered for further studies (see Table 1). The mass spectrometry proteomics data have

657 been deposited to the ProteomeXchange Consortium via the PRIDE partner repository.

658

659 **Bioinformatics Analysis**

660 RNA secondary structure was analysed using the "mfold" program

661 (http://bioinfo.rpi.edu/applications/mfold/old/RNA), based on minimum free energy

662 calculation at 25^0C (51). The virus-host RPPI dataset was visualized using Cytoscape

663 (version 3.1.0) (24). NetworkAnalyzer plugin in Cytoscape was used to compute the

664 topological parameters and centrality measures of the network. Gene ontology "GO" and

665 Reactome pathway analysis was performed using the "Gene Set Enrichment Analysis" tool

666 [https://www.gsea-msigdb.org/gsea/index.jsp (26, 27)].

667

668 **SARS-CoV-2 infection**

669 SARS-CoV-2 was obtained from BEI Resources (NR-52281, SARS-related coronavirus 2

670 isolate ISA-WA1/2020), amplified in Vero E6 cells in the BSL3 facility of THSTI, India,

671 titrated and stored frozen in aliquots. For SARS-CoV-2 infection studies, 200 μl of stock virus

672 was diluted in serum free media to 2000 TCID50/ml and added to Vero E6/ Huh7 cell

673 monolayer (seeded in 24 well plate) for 1 hour at 37^0C, supplemented with 5% CO_2. One

674 hour post-incubation, the infection medium was removed, cells were washed twice with 500

675 μl of serum free media and fresh DMEM+10% FBS was added. In case of plasmid over

676 expression or siRNA transfection study, cells were transfected with respective DNA or

677 siRNA 24 hours prior to infection with SARS-CoV-2. In case of 3-MA treatment, 5mM (final

678 concentration) 3-MA was added to the culture medium during infection, again added to the

679 complete medium after removing the infection medium and maintained for 48 hours,

680 followed by collection of culture medium and cells and subsequent experiments.

681

682 **Fluorescence *In Situ* Hybridization (FISH)**

683 *Preparation of RNA probe:*

684 Sequence corresponding to the 5'-300 bases of SARS-CoV-2 was PCR amplified from pUC57

685 vector and cloned into the pJet1.2 vector (Thermo Fisher Scientific, Massachusetts, USA)

686 under the control of T7 promoter. pJet1.2_5'-300 plasmid was linearized by restriction

687 digestion with XbaI. DIG-11-UTP (Cat no. 11209256910, Roche, Basel) labeled RNA was *in*

688 *vitro* synthesized using Maxi script *in vitro* transcription kit (Thermo Fisher Scientific,

689 Massachusetts, USA), following manufacturer's instruction. Template DNA was removed by

690 treatment with Dnase I, followed by precipitation of RNA using LiCl. An aliquot of the probe

691 was resolved by agarose gel electrophoresis to monitor its size and integrity.

692 *Fluorescence in situ hybridization:*

693 FISH was done as described with minor modifications in which, Tyramide super boost kit

694 (Cat No. B40933, Thermo Fisher Scientific, Massachusetts, USA) was used to detect the

695 fluorescence signal (52). In summary, Vero E6 Cells were seeded at 70-80% confluency on

696 coverslip overnight. Next day, cells were infected with the SARS-CoV-2 (see SARS-CoV-2

697 infection section) and incubated for 24 or 48 hours. Next, cells were washed three times in

698 PBS, followed by fixation in 4% Paraformaldehyde for 10 min at room temp. Cells were

21

699   rehydrated in 2xSSC buffer (300mM NaCl, 30mM Sodium Citrate) for 10 min at room temp,

700   followed by incubation with 50% formamide in 2xSSC buffer for 30 min at room temp. Next,

701   coverslips were washed four times with warm hybridization buffer (10% formamide in

702   2xSSC, warmed to 70^0C), followed by incubation with hybridization buffer containing 2 ng/μl

703   of probe for 3 days at 42^0C in a humified incubator. Cells were washed two times with

704   4xSSC buffer for 10min each, at 42^0C and incubated with 20ug/ml RNase A in 2xSSC buffer

705   for 30min at 37^0C. Next, cells were washed once with 2xSSC buffer and once with 0.1xSSC

706   buffer for 10 min at 42^0C. Endogenous peroxidase activity was quenched by adding 50 μl

707   3% H_2O_2 solution (provided in the Tyramide super boost kit) and incubating at room temp for

708   1 hour. Next, cells were blocked in 4% BSA (in PBS) for 1 hour at room temp, followed by

709   incubation with anti-LAMP2 (1:50 dilution) and biotin conjugated anti-DIG antibody (1:200

710   dilution) prepared in 4% BSA in PBST (PBS+ 0.2% Tween-20) for overnight at 4^0C. Next day

711   cells were washed three times in PBS (10 min each) and incubated with HRP-conjugated

712   streptavidin (provided in the Tyramide super boost kit) for 60 min at room temp. Next, cells

713   were washed three times in PBS and incubated with Goat-anti rabbit IgG Alexa Fluor 488

714   (1:1000 dilution, prepared in 4% BSA+PBS+ 0.1% Tween 20) for 1 hour at room temp. Cells

715   were washed three times in PBS. Next, freshly prepared Tyramide working solution was

716   added to the cells and incubated for 5 min at room temp, followed by addition of stop

717   solution (provided with the Tyramide super boost kit) and incubation for 3 min. Next, cells

718   were washed three times in PBS and coverslips were mounted on slide using antifade gold.

719   Images were acquired using a 100X objective in a confocal microscope (Olympus FV3000)

720   and analysed by Image lab FIJI software.

721

722   **RNA isolation and quantitative real time PCR (QRT-PCR) assay**

723   Intracellular RNA was isolated using TRI reagent (MRC, Massachusetts, USA), followed by

724   reverse transcription (RT) using Firescript cDNA synthesis kit (Solis Biodyne, Estonia). RNA

725   from culture medium was isolated using Qiagen viral RNA mini kit (Qiagen, Germany),

726   followed by reverse transcription (RT) using Firescript cDNA synthesis kit (Solis Biodyne,

727   Estonia). Random hexamers were used in cDNA synthesis. SYBR green based QRT-PCR

728   was done as described earlier (50). Following primers were used: SCoV2 QPCR FP: 5'-

729   TGGACCCCAAAATCAGCGAA, SCoV2 QPCR RP: 5'-TCGTCTGGTAGCTCTTCGGT; RP

730   II FP: 5'-GCACCACGTCCAATGACAT, RP II RP: 5'-GTCGGCTGCTTCCATAA, RP FP: 5'-

731   AGATTTGGACCTGCGAGCG, RP RP: 5'-GAGCGGCTGTCTCCACAAGT. Taqman based

732   QRT-PCR was done as described earlier, following the protocol suggested by Centre for

733   Disease Control, USA (53). Following primers and probes were used. N1 FP: 5'-

734   GACCCCAAAATCAGCGAAAT, N1 RP: 5'-TCTGGTTACTGCCAGTTGAATCTG, N1 Probe:

22

735   5'-FAM-ACCCCGCATTACGTTTGGTGGACC-BHQ1, N2 FP: 5'-

736   TTACAAACATTGGCCGCAAA, N2 RP: 5'-GCGCGACATTCCGAAGAA, N2 Probe: 5'-FAM-

737   ACAATTTGCCCCCAGCGCTTCAG-BHQ1; RP FP: 5'-AGATTTGGACCTGCGAGCG, RP

738   RP: 5'-GAGCGGCTGTCTCCACAAGT, RP Probe: 5'-FAM-

739   TTCTGACCTGAAGGCTCTGCGCG-BHQ1. Absolute quantification was used in SYBR

740   green QRT-PCRs. Standard plot was generated by serial dilution of known quantity of

741   template. SCoV2 PCR values were normalized to that of RNA Polymerase II (RP II,

742   intracellular RNA) or RNAse P (RP, culture medium RNA).

743

744   **Statistics**

745   Data are represented as mean±SEM of three experiments. P values were calculated using

746   two-tailed student t-Test (paired two sample for means).

747

748   **Immunofluorescence assay (IFA)**

749   Confocal imaging was performed as described (50). In brief, Huh7 and Vero E6 cells were

750   fixed with 4% Paraformaldehyde for 10 min at room temp, followed by incubation in blocking

751   buffer (4% BSA in PBS) for 1 hour at room temp and incubation with Lamp2 and LC3b

752   antibodies (1:50 and 1:50 dilution, respectively) in antibody dilution buffer (3% BSA in

753   PBS+0.1% Tween-20) for 16 hours, at 4^0C. Coverslips were washed three times in PBS,

754   followed by incubation with 1:500 dilution of goat anti-rabbit Alexa Fluor 488 and 1:500

755   dilution of goat anti-mouse Alexa Fluor 647 antibodies (Thermo Fisher Scientific,

756   Massachusetts, USA) in antibody dilution buffer at room temp for 1 hour. Coverslips were

757   washed three times in PBS and mounted on glass slides using antifade gold reagent

758   (Thermo Fisher Scientific, Massachusetts, USA). Images were acquired using a 60X

759   objective in a confocal microscope (Olympus FV3000) and analysed by Image lab FIJI

760   software.

761

762   **Western blot assay**

763   Samples were resolved by SDS-PAGE, transferred to 0.4μ PVDF membrane. Membranes

764   were blocked for 1 hour at room temp using 5% skimmed milk (in PBS). Next, membranes

765   were incubated with primary antibody overnight in PBST (PBS+0.05% Tween-20) + 5%

766   skimmed milk at 4^0C. Blots were washed 3 times in PBST, followed by incubation with HRP-

767   tagged secondary antibody at room temp for 1 hour. Blots were washed 3 times in PBST

768   and protein bands were visualized by enhanced chemiluminescence using a commercially

769   available kit (Bio Rad, California, USA).

770

References

1. Xu X, Chen P, Wang J, Feng J, Zhou H, Li X et al. Evolution of the novel coronavirus from the ongoing Wuhan outbreak and modeling of its spike protein for risk of human transmission. Sci China Life Sci 2020; 63(3): 457-460. https://doi.org/10.1007/s11427-020-1637-5 PMID: 32009228

2. Wu J, Yuan X, Wang B, Gu R, Li W, Xiang X et al. Severe Acute Respiratory Syndrome Coronavirus 2: From Gene Structure to Pathogenic Mechanisms and Potential Therapy. Front Microbiol 2020; 11: 1576. https://doi.org/10.3389/fmicb.2020.01576 PMID: 32719672

3. Hu B, Guo H, Zhou P, Shi ZL. Characteristics of SARS-CoV-2 and COVID-19. Nat Rev Microbiol 2020: 1-14. https://doi:10.1038/s41579-020-00459-7 PMID: 33024307

4. Trottein F, Sokol H. Potential Causes and Consequences of Gastrointestinal Disorders during a SARS-CoV-2 Infection. Cell Rep 2020; 32(3): 107915. https://doi.org/10.1016/j.celrep.2020.107915 PMID: 32649864

5. Decaro N, Lorusso A. Novel human coronavirus (SARS-CoV-2): A lesson from animal coronaviruses. Vet Microbiol 2020; 244: 108693. https://doi.org/10.1016/j.vetmic.2020.108693 PMID: 32402329

6. Wang Y, Grunewald M, Perlman S. Coronaviruses: An Updated Overview of Their Replication and Pathogenesis. In: Maier H, Bickerton E, editors. Coronaviruses methods in Molecular Biology. Springer-Verlag; 2020. Vol.1282, pp.1-29.

7. Sola I, Mateos-Gomez PA, Almazan F, Zunniga S, Enjuanes L. RNA-RNA and RNA-protein interactions in coronavirus replication and transcription, RNA Biol. 2011; 8: 237-248. https://doi.org/10.4161/rna.8.2.14991 PMID: 21378501

8. Yang D, Leibowitz JL. The Structure and Functions of Coronavirus Genomic 3' and 5' Ends. Virus Res 2015; 206: 120–133. https://doi.org/10.1016/j.virusres.2015.02.025 PMID: 25736566

9. Rangan R, Zheludev IN, Hagey RJ, Pham EA, Wayment-Steele HK, Glenn JS et al. RNA genome conservation and secondary structure in SARS-CoV-2 and SARS-

814   related viruses: a first look. RNA 2020; 26: 937-959.
815   https://doi:10.1261/rna.076141.120 PMID: 32398273
816   10. Miao Z, Tidu A, Eriani G, Martin F. Secondary structure of the SARS-CoV-2 5'-UTR.
817   RNA Boil 2020; 12: 1-10. https://doi.org/10.1080/15476286.2020.1814556
818   PMID: 32965173
819   11. Sola I, Almazan F, Zuniga S, Enjuanes L. Continuous and discontinuous RNA
820   synthesis in coronaviruses. Annu Rev Virol 2015; 2(1): 265-288.
821   http://doi.org/10.1146/annurev-virology-100114-055218 PMID: 26958916
822   12. Liu P, Li L, Millership JJ, Kang H, Leibowitz JL, Giedroc DP. A U-turn motif-
823   containing stem-loop in the coronavirus 5' untranslated region plays a functional role
824   in replication. RNA 2007; 13: 763–780. http://doi.org/10.1261/rna.261807 PMID:
825   17353353
826   13. Goebel SJ, Miller TB, Bennett CJ, Bernard KA, Masters PS. A hypervariable region
827   within the 3' cis-acting element of the murine coronavirus genome is nonessential for
828   RNA synthesis but affects pathogenesis. J Virol 2007; 81(3): 1274–1287.
829   http://doi.org/10.1128/JVI.00803-06 PMID: 17093194
830   14. Li H, Zhang X, Duncan R, Comai L, Lai MM. Heterogeneous nuclear
831   ribonucleoprotein A1 binds to the transcription-regulatory region of mouse hepatitis
832   virus RNA. Proc Natl Acad Sci U S A 1997; 94(18): 9544-9549.
833   https://doi.org/10.1073/pnas.94.18.9544 PMID: 9275159
834   15. Li H, Huang P, Park S, Lai MM. Polypyrimidine tract-binding protein binds to the
835   leader RNA of mouse hepatitis virus and serves as a regulator of viral transcription. J
836   Virol 1999; 73(1): 772-777. http://doi.org/10.1128/JVI.73.1.772-777.1999 PMID:
837   9847386
838   16. Choi KS, Huang PY, Lai MM. Polypyrimidine-tract-binding protein affects
839   transcription but not translation of mouse hepatitis virus RNA. Virology 2002 303(1):
840   58-68. https://doi.org/10.1006/viro.2002.1675 PMID: 12482658
841   17. Fung TS, Liu DX. Human coronavirus: host-pathogen interaction. Annu Rev microbiol
842   2019; 73: 529-557. https://doi.org/10.1146/annurev-micro-020518-115759
843   PMID: 31226023
844   18. Huang P, Lai MM. Heterogeneous nuclear ribonucleoprotein a1 binds to the 3′-
845   untranslated region and mediates potential 5′-3′-end cross talks of mouse hepatitis
846   virus RNA. J Virol 2001; 75: 5009-5017. http://doi.org/10.1128/JVI.75.11.5009-
847   5017.2001 PMID: 11333880
848   19. Nanda SK, Johnson RF, Liu Q, Leibowitz JL. Mitochondrial HSP70, HSP40, and
849   HSP60 bind to the 3′ untranslated region of the murine hepatitis virus genome. Arch
850   Virol 2003; 149: 93-111. https://doi.org/10.1007/s00705-003-0196-4 PMID: 14689278
851   20. Ramanathan M, Majzoub K, Rao DS, Neela PH, Zarnegar BJ, Mondal S et al. RNA–
852   protein interaction detection in living cells. Nat Methods 2018; 15(3): 207.
853   https://doi.org/10.1038/nmeth.4601 PMID: 29400715
854   21. Kall L, Storey JD, MacCoss MJ, Noble WS. Posterior error probabilities and false
855   discovery rates: two sides of the same coin. J Proteome Res 2008; 7(1): 40-44.
856   https://doi.org/10.1021/pr700739d PMID: 18052118
857   22. Cao D, Meng XJ. Molecular biology and replication of hepatitis E virus. Emerg
858   Microbes Infect 2020; 1(8): 1-10. https://doi.org/10.1038/emi.2012.7 PMID: 26038426
859   23. Schmidt N, Lareau CA, Keshishian H, Melanson R, Zimmer M, Kirschner L, et al. A
860   direct RNA-protein interaction atlas of the SARS-CoV-2 RNA in infected human cells.
861   BioRxiv [Preprint]. 2020 bioRxiv 204404 [posted 2020 july 15; cited 2020 dec 14]: [33

862   p.]. Available from: https://www.biorxiv.org/content/10.1101/2020.07.15.204404v1
863   doi: htpp://doi.org/10.1101/2020.07.15.204404.
864
865 24. Cline MS, Smoot M, Cerami E, Kuchinsky A, Landys N, Workman C et al.
866   Integration of biological networks and gene expression data using Cytoscape. Nat
867   protoc 2007; 2(10): 2366-2382. https://doi.org/10.1038/nprot.2007.324 PMID:
868   17947979
869 25. Gordon DE, Jang GM, Bouhaddou M, Xu J, Obernier K, O'Meara MJ et al. A SARS-
870   CoV-2-Human Protein-Protein Interaction Map Reveals Drug Targets and Potential
871   Drug-Repurposing. Nature 2020; 583(7816): 459–468.
872   https://doi.org/10.1038/s41586-020-2286-9 PMID: 32353859
873 26. Subramanian A, Tamayo P, Mootha VK, Mukherjee S, Ebert BL, Gillette MA et al.
874   Gene set enrichment analysis: a knowledge-based approach for interpreting
875   genome-wide expression profiles. Proc Natl Acad Sci U S A 2005; 102(43): 15545-
876   15550. https://doi.org/10.1073/pnas.0506580102 PMID: 16199517
877 27. Mootha VK, Lindgren CM, Eriksson KF, Subramanian A, Sihag S, Lehar J et al.
878   PGC-1α-responsive genes involved in oxidative phosphorylation are coordinately
879   downregulated in human diabetes. Nat Genet 2003; 34(3): 267-73.
880   https://doi.org/10.1038/ng1180 PMID: 12808457
881 28. Chen C, Qi F, Shi K, Li Y, Li J, Chen Y et al. Thalidomide combined with low-dose
882   short-term glucocorticoid in the treatment of critical Coronavirus Disease 2019. Clin
883   Transl Med 2020; 10(2): e35. https://doi.org/10.1002/ctm2.35 PMID: 32508009
884 29. Acosta-Elias J, Espinosa-Tanguma R. The Folate Concentration and/or Folic Acid
885   Metabolites in Plasma as Factor for COVID-19 Infection. Front pharmacol 2020; 11:
886   1062. https://doi.org/10.3389/fphar.2020.01062 PMID: 32765270
887 30. Matsuyama S, Kawasea M, Naoa N, Shiratoa K, Ujikeb M, Kamitanic W et al. The
888   inhaled steroid ciclesonide blocks SARS-CoV-2 RNA replication by targeting the viral
889   replication-transcription complex in cultured cells. J Virol 2020;
890   http://doi.org/10.1128/JVI.01648-20 PMID: 33055254
891 31. Bello-Perez M, Sola I, Novoa B, Klionsky DJ, Falco A. Canonical and noncanonical
892   autophagy as potential targets for COVID-19. Cells 2020; 9(7):
893   1619. https://doi.org/10.3390/cells9071619 PMID: 32635598
894 32. Takayama K. In vitro and Animal Models for SARS-CoV-2 research. Trends
895   Pharmacol. Sci 2020; 41(8): 513-517. https://doi.org/10.1016/j.tips.2020.05.005
896   PMID: 32553545
897 33. Gough NR, Hatem CL, Fambrough DM. The family of LAMP-2 proteins arises by
898   alternative splicing from a single gene: characterization of the avian LAMP-2 gene
899   and identification of mammalian homologs of LAMP-2b and LAMP-2c. DNA Cell Biol
900   1995; 14(10): 863-867. https://doi.org/10.1089/dna.1995.14.863 PMID: 7546292
901 34. Endo Y, Furuta A, Nishino I. Danon disease: a phenotypic expression of LAMP-2
902   deficiency. Acta Neuropathol 2015; 129(3): 391–398.
903   https://doi.org/10.1007/s00401-015-1385-4 PMID: 25589223
904 35. Sansanwal P, Yen B, Gahl WA, Ma Y, Ying L, Wong LJC et al. Mitochondrial
905   autophagy promotes cellular injury in nephropathic cystinosis. J Ame Soc Neph
906   2010; 21(2): 272-283. https://doi.org/10.1681/ASN.2009040383 PMID: 19959713
907 36. Zust R, Miller TB, Goebel SJ, Thiel V, Masters PS. Genetic interactions between an
908   essential 3′ cis-acting RNA pseudoknot, replicase gene products, and the extreme 3′
909   end of the mouse coronavirus genome. J Virol 2008; 82(3): 1214-1228.
910   https://doi.org/10.1128/JVI.01690-07 PMID: 18032506

37. Kabrane-Lazizi Y, Meng XJ, Purcell RH, Emerson S U. Evidence that the genomic RNA of hepatitis E virus is capped. J Virol 1999; 73(10): 8848–8850. https://doi.org/10.1128/JVI.73.10.8848-8850.1999 PMID: 10482642

38. Ran R, Lu A, Xu H, Tang Y, Sharp FR. Heat-Shock Protein Regulation of Protein Folding, Protein Degradation, Protein Function, and Apoptosis. In: Lajtha A, Chan PH, editors. Handbook of Neurochemistry and Molecular Neurobiology, Springer; 2007. pp.89-107.

39. Mine A, Hyodo K, Tajima Y, Kusumanegara K, Taniguchi T, Kaido M et al. Differential roles of Hsp70 and Hsp90 in the assembly of the replicase complex of a positive-strand RNA plant virus. J Virol 2012; 86(22): 12091-12104. https://doi.org/10.1128/JVI.01659-12 PMID: 22933272

40. Ma Z, Moore R, Xu X, Barber GN. DDX24 negatively regulates cytosolic RNA-mediated innate immune signaling. PLoS pathog 2013; 9(10): e1003721. https://doi.org/10.1371/journal.ppat.1003721 PMID: 24204270

41. Li JY, Liao CH, Wang Q, Tan YJ, Luo R, Qiu Y, et al. The ORF6, ORF8 and nucleocapsid proteins of SARS-CoV-2 inhibit type I interferon signaling pathway. Virus res 2020; 286: 198074. https://doi.org/10.1016/j.virusres.2020.198074 PMID: 32589897

42. TianY, Han X, Tian DL. The biological regulation of ABCE1. IUBMB life 2012; 64(10): 795-800. https://doi.org/10.1002/iub.1071 PMID: 23008114

43. Solomentsev G, Diehl C, Akke M. Conformational entropy of fk506 binding to fkbp12 determined by nuclear magnetic resonance relaxation and molecular dynamics simulations. Biochemistry 2018; 57(9): 1451-1461. https://doi.org/10.1021/acs.biochem.7b01256 PMID: 29412644

44. White JP, Lloyd RE. Regulation of stress granules in virus systems. Trends microbiol 2012; 20(4): 175–183. https://doi.org/10.1016/j.tim.2012.02.001 PMID: 22405519

45. Cuervo AM, Dice JF. Unique properties of lamp2a compared to other lamp2 isoforms. J cell sci 2000; 113(24): 4441-4450. PMID: 11082038

46. Mohamud Y, Shi J, Qu J, Poon T, Xue YC, Deng H, et al. Enteroviral infection inhibits autophagic flux via disruption of the SNARE complex to enhance viral replication. Cell rep 2018; 22(12): 3292-3303. https://doi.org/10.1016/j.celrep.2018.02.090 PMID: 29562184

47. Jones-Jamtgaard KN, Wozniak AL, Koga H, Ralston R, Weinman SA. Hepatitis C virus infection increases autophagosome stability by suppressing lysosomal fusion through an Arl8b-dependent mechanism. J Biol Chem 2019; 294(39): 14257-14266. https://doi.org/10.1074/jbc.RA119.008229 PMID: 31383738

48. Hase K, Fujiwara Y, Kikuchi H, Aizawa S, Hakuno F, Takahashi SI, et al. RNautophagy/DNautophagy possesses selectivity for RNA/DNA substrates. Nucleic Acids Res. 2015; 43(13): 6439-6449. https://doi.org/10.1093/nar/gkv579 PMID: 26038313

49. Fujiwara Y, Furuta A, Kikuchi H, Aizawa S, HatanakaY, Konya C, et al. Discovery of a novel type of autophagy targeting RNA. Autophagy 2013; 9(3): 403–409. https://doi.org/10.4161/auto.23002 PMID: 23291500

50. Nair VP, Anang S, Subramani C, Madhvi A, Bakshi K, Srivastava A et al. Endoplasmic reticulum stress induced synthesis of a novel viral factor mediates efficient replication of genotype-1 hepatitis E virus. PLoS pathog. 2016; 12 (4): e1005521. https://doi.org/10.1371/journal.ppat.1005521 PMID: 27035822

958 51. Zuker M. Mfold web server for nucleic acid folding and hybridization
959   prediction. Nucleic Acids Res. 2003; 31(13): 3406-3415.
960   https://doi.org/10.1093/nar/gkg595 PMID: 12824337
961 52. Ying S, Kay AB. The technique of in situ hybridization. In: Rogers DF, Donnelly LE,
962   editors. Human Airway Inflammation part of Methods in Molecular Medicine book
963   series. Springer protocol; 2001. Vol.56. pp. 263-283.
964 53. Mittal A, Gupta A, Kumar S, Surjit M, Singh B, Soneja M et al. Gargle lavage as a
965   viable alternative to swab for detection of SARS-CoV-2. IJMR. 2020; 152(1): 77-81.
966   https://doi.org/10.4103/ijmr.IJMR_2987_20 PMID: 32820725

967
968
969
970
971
972
973
974
975
976
977
978
979
980
981
982
983
984
985
986
987
988
989
990
991
992
993
994
995
996

Figure legends

Figure 1. Establishment of RaPID assay to identify the host interaction partners of SARS-CoV-2 5'-300 and 3'-203 RNA.

   A. Schematic of predicted secondary structure of SARS-CoV-2 5'-300 RNA. "*" denotes an unannotated stem loop in the 5'-UTR.

   B. Schematic of predicted secondary structure of SARS-CoV-2 3'-203 RNA.

   C. Schematic of RaPID assay workflow. Biotin is represented as 'B', agarose is represented as 'A' and streptavidin is represented as 'S'.

   D. Western blot detection of BirA ligase and GAPDH level in HEK293T cells transfected with the RaPID plasmid for 48 hours.

   E. Western blot detection of Biotinylated protein in HEK293T cells transfected with BirA ligase and treated with Biotin for different time points, as indicated.

   F. Western blot detection of CUGBP1 protein in the whole cell extract of HEK293T cells (WCE) and in streptavidin agarose pull down of EDEN 15 RNA interacting biotinylated proteins.

Figure 2. Identification of SARS-CoV-2 5'-300 and 3'-203 RNA interacting host proteins by RaPID assay.

   A. Clustering analysis of correlation between biological replicates used in LC-MS-MS.

   B. Venny analysis of 5'-300 and 3'-203 RNA interacting proteins. (3'-203 in red, 3'-203_Biotin in blue, 5'-300 in green, 5'-300_Botin in yellow, pRMB in brown and pRMB_Biotin in dark green).

   C. Schematic of RNA-protein interaction network of the 3'-203 SARS-CoV-2 RNA. Black node: 3'-203; Red node: Host protein. Host proteins that interact with each other contain green color inside the node.

   D. Schematic of RNA-protein interaction network of the 5'-300 SARS-CoV-2 RNA. Black node: 5'-300; Blue node: Host protein. Host proteins that interact with each other contain yellow color inside the node.

   E. Schematic of RNA-protein interaction network of the 5'-300+3'-203 SARS-CoV-2 RNAs. Black nodes: 5'-300 or 3'-203; Blue or red nodes: Host protein. Host proteins that interact with each other contain yellow or green color inside the node. Common host proteins that interact with both 5'-3000 and 3'-203 RNA are represented with dual (red+blue) color.

Figure 3. Lamp2 associates with the 5'-end of the SARS-CoV-2 genome and modulates the level of viral RNA in infected Vero E6 cells.

29

1033   A. Immunofluorescence staining of Nucleocapsid Protein (red) and nucleus (blue) in
1034   SARS-CoV-2 infected Vero E6 cells, 48 hour post-infection.

1035   B. Western blot detection of Nucleocapsid protein (upper image) and GAPDH (lower
1036   image) in SARS-CoV-2 infected Vero E6 cells, 48 hour post-infection.

1037   C. Level of SARS-CoV-2 RNA [normalized to that of RNase P (RP)] in the culture
1038   medium (secreted) and inside Vero E6 cells (intracellular) that are infected with the
1039   SARS-CoV-2 for the indicated periods. Real-time PCR reactions were performed
1040   using SYBR green based protocol. Data are mean $\pm$ SEM.

1041   D. Intracellular level of SARS-CoV-2 RNA in Vero E6 cells that are infected with SARS-
1042   CoV-2 for the indicated periods. Real-time PCR reactions were performed using
1043   Taqman probe-based protocol. N1, N2 and RP represents two regions within the
1044   SARS-CoV-2 Nucleocapsid coding region and one region within RNase P (RP) that
1045   was selected for PCR amplification. Data are mean $\pm$ SEM.

1046   E. Fluorescence *in situ* hybridization of SARS-CoV-2 5'-300 RNA and Lamp2, at
1047   indicated periods, post-infection. Lamp2 protein, SARS-CoV-2 RNA and Nucleus is
1048   denoted by green, red and blue, respectively. Scale bar is 20μM.

1049   F. Western blot detection of Lamp2 (Lamp2 antibody, upper panel) and GAPDH (lower
1050   panel) proteins in Vero E6 cells transfected for 72 hours with non targeting (NT)
1051   SiRNA or Lamp2 siRNA.

1052   G. Level of SARS-CoV-2 RNA (normalized to that of RP) in the culture medium of Vero
1053   E6 cells transfected with NT siRNA or Lamp2 siRNA and infected with SARS-CoV-2
1054   for 48 hours. Data are mean $\pm$ SEM.

1055   H. Intracellular level of SRS CoV2 RNA (normalized to that of RP II) in Vero E6 cells
1056   treated with Lamp2 SiRNA and infected with SARS-CoV-2 for 48 hours. Data are
1057   mean $\pm$ SEM.

1058

1059   **Figure 4. Lamp2 modulates viral RNA level in SARS-CoV-2 infected cells.**

1060   A. Western blot detection of Lamp2a protein level [using anti-HA antibody (upper panel)
1061   and anti-Lamp2 antibody (middle panel)] and GAPDH protein level (lower panel) in
1062   mock transfected or pcDNA Lamp2a transfected Vero E6 Cells.

1063   B. Western blot detection of Lamp2b protein level using anti-Lamp2 antibody (upper
1064   panel) and GAPDH protein level (lower panel) in mock transfected or pcDNA
1065   Lamp2b transfected Vero E6 Cells.

1066   C. Western blot detection of Lamp2c protein level using anti-Lamp2 antibody (upper
1067   panel) and GAPDH protein level (lower panel) in mock transfected or pcDNA Lamp2c
1068   transfected Vero E6 Cells.

1069   D. Intracellular level of SRS CoV2 RNA (normalized to that of RP II) in Vero E6 cells

1070   transfected with the indicated plasmids and infected with SARS-CoV-2 for 48 hours.

1071   Data are mean ± SEM.

1072   E. Level of SARS-CoV-2 RNA (normalized to that of RP) in the culture medium of Vero

1073   E6 cells transfected with the indicated plasmids and infected with SARS-CoV-2 for

1074   48 hours. Data are mean ± SEM.

1075   F. Western blot detection of Lamp1 protein level using Lamp1 antibody (upper panel)

1076   and GAPDH protein level (lower panel) in Huh7 cells transfected for 72 hours with

1077   non targeting SiRNA or Lamp1 SiRNA.

1078   G. Level of SARS-CoV-2 RNA (normalized to that of RP) in the culture medium of Huh7

1079   cells transfected with Lamp1 SiRNA (72 hours) and infected with SARS-CoV-2 for 48

1080   hours. Data are mean ± SEM.

1081   H. Level of SARS-CoV-2 RNA (normalized to that of RP II) in the culture medium of

1082   Huh7 cells transfected with Lamp1 SiRNA (72 hours) and infected with SARS-CoV-2

1083   for 48 hours. Data are mean ± SEM.

1084

1085   **Figure 5. Increased Lamp2 and LC3-II levels in SARS-CoV-2 infected Vero E6 and**

1086   **Huh7 cells do not promote autophagolysosome formation.**

1087   A. Western blot detection of indicated proteins in SARS-CoV-2 infected Vero E6 and

1088   Huh7 cells, 48 hour post-infection.

1089   B. Level of SARS-CoV-2 RNA (normalized to that of RP) in the culture medium of Vero

1090   E6 cells infected with SARS-CoV-2 and treated with 5mM 3MA for 48 hour. Data are

1091   mean ± SEM.

1092   C. Intracellular level of SRS CoV2 RNA (normalized to that of RP II) in Vero E6 cells

1093   treated with 5mM 3MA for 48 hour. Data are mean ± SEM.

1094   D. Level of SARS-CoV-2 RNA (normalized to that of RP) in the culture medium of Huh7

1095   cells infected with SARS-CoV-2 and treated with 5mM 3MA for 48 hour. Data are

1096   mean ± SEM.

1097   E. Intracellular level of SRS CoV2 RNA (normalized to that of RP II) in Huh7 cells

1098   treated with 5mM 3MA for 48 hour. Data are mean ± SEM.

1099   F. Immunofluorescence staining of Lamp2 (green), LC3 (red), and nucleus (blue), in

1100   uninfected or 48 hour SARS-CoV-2 infected Vero E6 cells. Yellow indicates

1101   colocalization of the red and green signals. Scale bar is 20μM.

1102

1103

1104

Legend to supplementary figures

S1 Figure. Schematic of predicted secondary structure of SARS-CoV-2 5'-300 RNA.

    A. Schematic of predicted secondary structure of SARS-CoV-2 5'-300 RNA. "*" denotes an unannotated stem loop in the 5'-UTR.

    B. Schematic of predicted secondary structure of SARS-CoV-2 5'-300 RNA + SL-A+ SL-B hybrid RNA.

S2 Figure. **Schematic of predicted secondary structure of SARS-CoV-2 3'-203 RNA.**

    A. Schematic of predicted secondary structure of SARS-CoV-2 3'-203 RNA.

    B. Schematic of predicted secondary structure of SARS-CoV-2 3'-203 RNA + SL-A + SL-B hybrid RNA.

S3 Figure. Normalized distribution curve of LC-MS-MS identified peptides.

    A. PEP score wise normal distribution of all peptides identified in LC-MS-MS in different biological replicates.

S4 Figure. **RPPI network of SARS-CoV-2 5'-300 RNA + 3'-203 RNA + PPI involved in virus replication.**

    A. Schematic of RPPI network of the 5'-300+3'-203 SARS-CoV-2 RNAs + PPI involved in virus replication. Black nodes: 5'-300 or 3'-203; Blue or red nodes: Host protein. Host proteins that interact with each other contain yellow or green color inside the node. Common host proteins that interact with both 5'-3000 and 3'-203 RNA are represented with dual (red+blue) color. Viral protein nodes are labeled. Host proteins involved in PPI with viral proteins are indicated in sky blue. Interaction among viral proteins is represented by blue lines.

    B. Schematic of PPI network involved in SARS-CoV-2 replication. Viral protein nodes are labeled. Host proteins involved in PPI with viral proteins are indicated in sky blue. Interaction among viral proteins is represented by blue lines.

S5 Figure. GO analysis of 5'-300 and 3'-203 SARS-CoV-2 RNA interacting proteins.

Proteins involved in top 10 biological processes are indicated in blue.

S6 Figure. Reactome pathway analysis of 5'-300 and 3'-203 SARS-CoV-2 RNA interacting proteins.

Proteins involved in top 10 pathways are indicated in blue.

32

1142 **S7 Figure. Lamp2 modulates viral RNA level in SARS-CoV-2 infected Huh7 cells.**

1143 A. Level of SARS-CoV-2 RNA [normalized to that of RNase P (RP II)] in the culture
1144   medium (secreted) and inside Huh7 cells (intracellular) that are infected with the
1145   SARS-CoV-2 for the indicated periods. Real-time PCR reactions were performed
1146   using SYBR green based protocol. Data are mean $\pm$ SEM.

1147 B. Western blot detection of SARS-CoV-2 nucleocapsid protein (upper panel) and
1148   GAPDH (lower panel) in SARS-CoV-2 infected Huh7 cells, 48 hour post-infection.

1149 C. Western blot detection of Lamp2 (Lamp2 antibody, upper panel) and GAPDH lower
1150   panel) protein in Huh7 cells transfected for 72 hours with NT SiRNA or Lamp2
1151   siRNA.

1152 D. Level of SARS-CoV-2 RNA (normalized to that of RP) in the culture medium of Huh7
1153   cells transfected with Lamp2 SiRNA and infected with SARS-CoV-2 for 48 hours.
1154   Data are mean $\pm$ SEM.

1155 E. Intracellular level of SARS-CoV-2 RNA (normalized to that of RP II) in Huh7 cells
1156   transfected with Lamp2 siRNA and infected with SARS-CoV-2 for 48 hours. Data are
1157   mean $\pm$ SEM.

1158 F. Western blot detection of Lamp2a protein level [using anti-HA antibody (upper panel)
1159   and anti-Lamp2 antibody (middle panel)] and GAPDH protein level (lower panel) in
1160   mock transfected or pcDNA Lamp2a transfected Huh7 Cells.

1161 G. Western blot detection of Lamp2b protein level [using anti-HA antibody (upper panel)
1162   and anti-Lamp2 antibody (middle panel)] and GAPDH protein level (lower panel) in
1163   mock transfected or pcDNA Lamp2b transfected Huh7 Cells.

1164 H. Western blot detection of Lamp2c protein level using anti-Lamp2 antibody (upper
1165   panel) and GAPDH protein level (lower panel) in mock transfected or pcDNA Lamp2c
1166   transfected Huh7 Cells.

1167 I. Level of SARS-CoV-2 RNA (normalized to that of RP) in the culture medium of Huh7
1168   cells transfected with indicated plasmids and infected with SARS-CoV-2 for 48 hours.
1169   Data are mean $\pm$ SEM.

1170 J. Intracellular level of SRS CoV2 RNA (normalized to that of RP II) in Huh7 cells
1171   transfected with indicated plasmids and infected with SARS-CoV-2 for 48 hours.
1172   Data are mean $\pm$ SEM.

1173

1174

1175

1176

1177

1178 **Supporting information**

1179

1180 S1 Fig. Schematic of predicted secondary structure of SARS-CoV-2 5'-300 RNA.

1181 S2 Fig. Schematic of predicted secondary structure of SARS-CoV-2 3'-203 RNA.

1182 S3 Fig. Normalized distribution curve of LC-MS-MS identified peptides.

1183 S4 Fig. RPPI network of SARS-CoV-2 5'-300 RNA + 3'-203 RNA + PPI involved in virus

1184 replication.

1185 S5 Fig. GO analysis of 5'-300 and 3'-203 SARS-CoV-2 RNA interacting proteins.

1186 S6 Fig. Reactome pathway analysis of 5'-300 and 3'-203 SARS-CoV-2 RNA interacting

1187 proteins.

1188 S7 Fig. Lamp2 modulates viral RNA level in SARS-CoV-2 infected Huh7 cells.

1189 S1 Table. List of host proteins that associate with SARS-CoV-2 5'-300 and 3'-203 RNA.

1190 S2 Table. Host proteins that interact with the 3'-end of HEV genome, identified by RaPID

1191 assay.

1192 S3 Table. Comparison of expression of prey proteins identified in RaPID assay in human

1193 Lungs and Intestine.

1194

34

Figure 1

A

SARS CoV2 5'-300 RNA

SL-IV

SL-III

SL-II

SL-I

SL-*

SL-Va

SL-Vc   SL-Vb

5'

3'

SL-A

SL-B

B

SL-II

SL-III

SARS CoV2 3'-203 RNA

SL-I

SL-IV

5'

3'

SL-A

SL-B

C

5'-300/3

BirA   BirA

SL A   SL B

↓ Biotin treatment

B B B

BirA   BirA

B   B

↓ Protease treatment

B   B
B

B
B

↓ Streptavidin agarose pull down

S
A
n

↓ LC-MS-MS

Protein identification

D

Mol Wt. (kDa)	Mock	RaPID Plasmid	
48			
35		←	BirA ligase
25			
48			
35		←	GAPDH
25			

E

Duration of biotin treatment (hours):	6	-	12	-	18	-
Biotin:	+	-	+	-	+	-
BirA:	+	+	+	+	+	+

75
63
48
35
25
20

Biotinylated proteins

Mol Wt. (kDa)

F

Biotin:	-	-	+	-	+
BirA:	-	-	-	+	+
EDEN15:	-	-	-	+	+

75
63
48
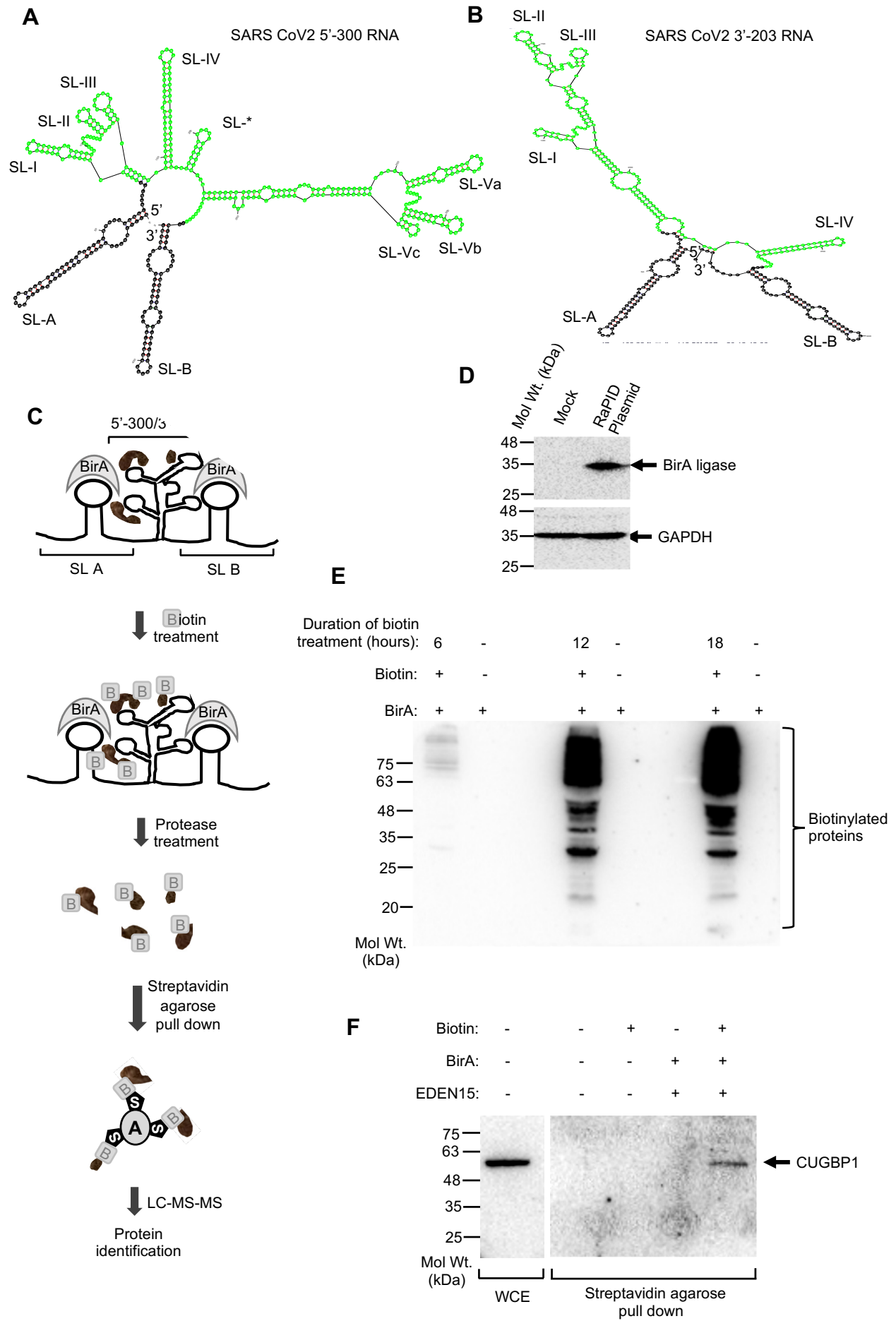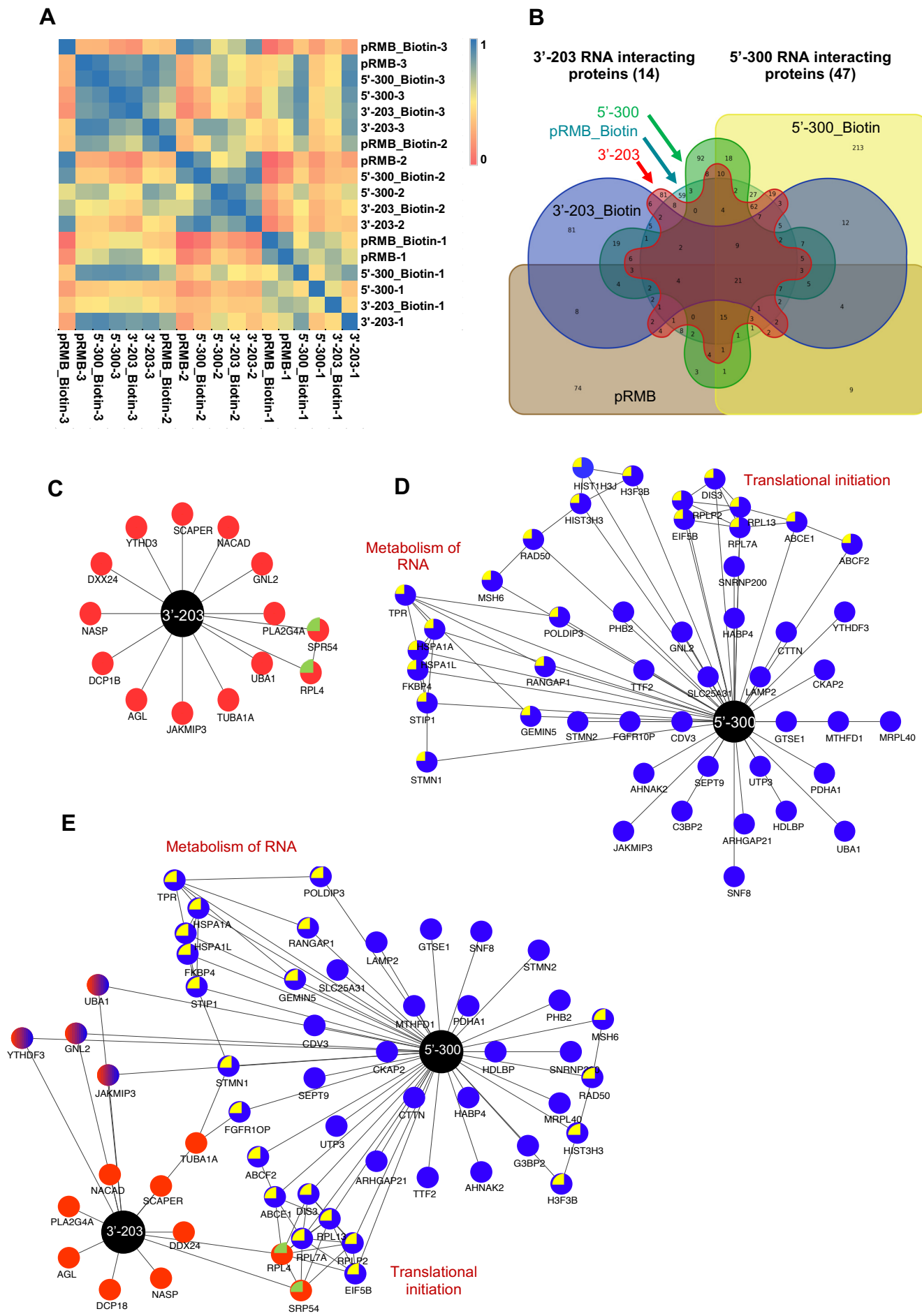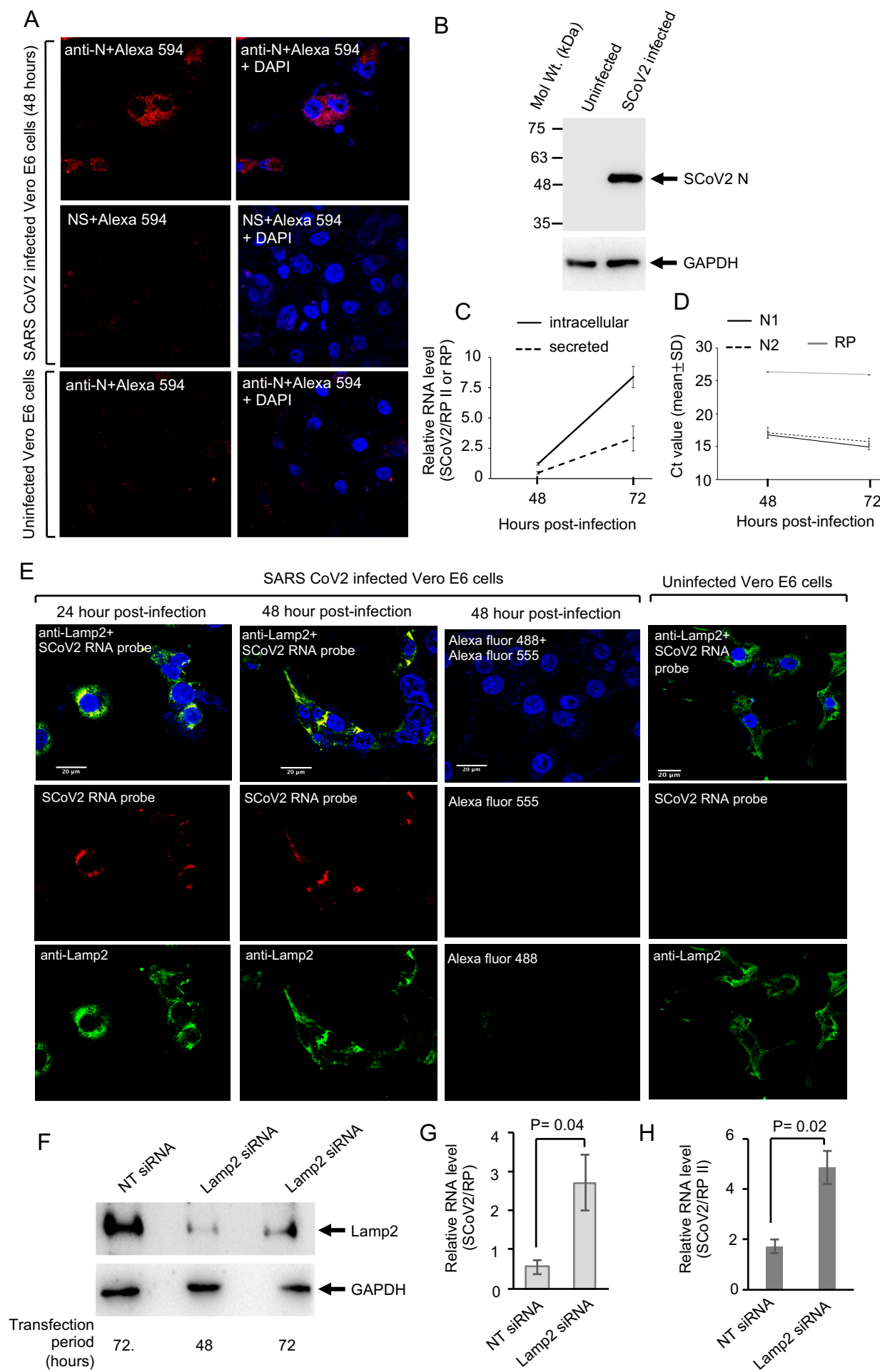35
25

← CUGBP1

Mol Wt. (kDa)

WCE   Streptavidin agarose pull down

Figure 2

Figure 3

Figure 4

Figure 5